2015년 2월

碩士學位論文

RhBMP-2 모방 펩타이드가 융합된 삼차원 폴리카프로락톤 스캐폴드에 대한 조골모세포의 생물학적 거동

조선대학교 대학원

치의생명공학과

신 건 수

RhBMP-2 모방 펩타이드가 융합된 삼차원 폴리카프로락톤 스캐폴드에 대한 조골모세포의 생물학적 거동

Biological behavior of preosteoblast cell on 3-D PCL scaffolds with integrated rhBMP-2 mimetic peptide

2015年 2月 25日

조선대학교 대학원

치의생명공학과

신 건 수

RhBMP-2 모방 펩타이드가 융합된 삼차원 폴리카프로락톤 스캐폴드에 대한 조골모세포의 생물학적 거동

지도교수 김 병 훈

이 논문을 공학 석사학위신청 논문으로 제출함.

2014年 10月

조선대학교 대학원

치의생명공학과

신 건 수

신건수의 석사학위 논문을 인준함

위원장 조선대학교 교수 고 영 무 印

위 원 전남대학교 교수 국 민 석 印

위 원 조선대학교 교수 김 병 훈 印

2014年 11月

조선대학교 대학원

CONTENTS

LIST OF TABLES

LIST OF FIGURES

국문초록

RhBMP-2 모방 펩타이드가 융합된 삼차원 폴리카프로락톤 스캐폴드에 대한 조골모세포의 생물학적 거동

Geon-Soo Shin
Advisor : Prof. Byung-Hoon Kim, Ph.D.
Department of Biodental Engineering
Graduate School of Chosun University

골 형성 단백질 (Bone Morphogenetic Protein, BMP)은 골 형성에 직접적으로 관여하는 강력한 유도인자로서 탈무기질골 (demineralized bone matrix, DBM)이 이소성 골 형성 (ectopic bone formation)을 유도한다는 사실을 발견하여 BMP라 명명하였으며, 형질전환증식인자 (TGF-β) super family군에 속한다.

이중에서 핵심 펩타이드 서열은 골 재생의 관점에서 BMP의 활성을 모방할 수 있다. BMP-2의 아미노산 서열 중 기능성을 나타낸다고 알려져 있는 부위의 일부 아미노산인 73~92 아미노산 서열을 재조합하여 BMP-2 peptide (P24)를 합성하였다. 이러한 기술을 이용한 생체모방형 펩타이드는 그 본래의 활성은 그대로 유지하면서도 분자량이 적고 구조가 간단하여 안정하면서 취급이 간편하다는 장점을 가지고 있다. 본 연구에서는 플라즈마 표면개질로 중합된 3차원 폴리카프로락톤 (Polycaprolactone, PCL) 스캐폴드에 P24 펩타이드의 고정화에 의한 조골모세포의 부착과 증식 그리고 분화에 미치는 영향을 평가하였다.

3-D PCL 스캐폴드는 PCL을 90℃에서 용융하였으며, 노즐의 크기 300 μm, 플로터의 속도 220 mm/min, 압력 580 ± 10 MPa 적층조건에서 기공 크기 150 μm, 각각의

층이 이루는 각도는 45° 이고, Fused Deposition Modeling (FDM) 방식으로 제작하였다. 저온 저압 RF 플라즈마 중합공정으로 PCL 스캐폴드 표면에 Poly acrylic acid (PAAc), Poly allylamine (PAAm), Poly 1,2-Diaminocyclohexane (DACH) 고분자박막을 코팅하였다. 중합처리 된 PCL 스캐폴드 표면 위에 P24 펩타이드를 고정화하여 표면 형상 및 조성을 FE-SEM (S-4800, Hitachi, Japan), ATR-FTIR (Nicolet 6700, Thermo electron, USA), XPS (VG Multilab 2000, ThermoVG Scientific, U.K), AFM (XE-100, Park systems, Korea)으로 분석하였으며, 플라즈마 세기에 따른 PCL 스캐폴드 표면에 존재하는 카르복실기와 아민기의 함량은 Toluidine Blue-O (TBO) 와 Methyl Orange (MO) 정량분석을 통하여 조사하였다. 시료표면의 친수성은 접촉각 (water contact angle, GS, Surface Tech Co. Ltd, Korea) 측정으로 확인하였다. 또한 조골모세포의 분화정도는 alkaline phosphatase (ALP)activity 활성도로 평가하였으며, 세포의 증식은 MTT assay, 세포 생존률과 독성평가를 하기 위하여 live/dead 염색법을 수행하였고, 세포형태를 확인하기 위하여 rhodamine-phalloidin 염색을 하였다. ATR-FTIR을 통해 아마이드 결합 및 아민기와 카르복실기가 존재함을 관찰하였으며, 샘플표면의 친수성은 아민기와 카르복실기 밀도에 영향을 미쳤다. PCL 표면에 rhBMP-2 모방 펩타이드가 고정화된 각각의 그룹은 FE-SEM, XPS 및 AFM을 이용하여 관찰한 결과, 형태와 위상학적인 변화를 관찰할 수 있었다. 이러한 결과를 바탕으로, 플라즈마 중합반응으로 도입한 아민기 및 카르복실기는 생체활성물질을 고정화하는데 있어서 적절한 표면을 제공해주며, rhBMP-2 모방 펩타이드가 고정화된 그룹은 조골모세포와의 생체적합성이 적절한 표면임을 알 수 있었다. 또한 이러한 방법들은 향후 골 조직공학 및 생체재료의 기술개발에 응용이 가능할 것으로 사료된다.

Chapter 1. Introduction

Biomaterials for tissue engineering and regenerative medicine should be both biodegradable and bioactive (Zuwei et. al, 2007). Various biomaterials are used in bone and teeth replacement. Depending on their properties and functions in the human body, the materials range from ceramics to metals and polymers (Chen and Thouas, 2015).

Polycaprolactone (PCL) is an FDA-approved bio-absorbable polymer for implantation in the human body. In addition, it was used as dental materials because of mechanical properties and excellent biocompatibility (Shuqiong et. al, 2014). PCL is bio-absorbable, biodegradable and has an excellent tensile strength. However, its application, particularly in tissue engineering, is hampered by its hydrophobicity, neutral charge distribution, slow degradation rate and reduced cell attachment/spreading (Wiens et. al, 2014).

Layered manufacturing methods or solid freeform fabrication technologies have being widely used for rapid prototyping (RP) purposes such as fabrication of complex shapes and models for visualization, verification and assembly purposes during product creation. In recent years, layered manufacturing has evolved from rapid prototyping techniques to rapid manufacturing methods where functional parts with tailored properties are produced for potential end use in a product (Kantaros and Karalekas, 2013). Various layered manufacturing techniques have been developed these include Stereo-Lithography, Fused Deposition Modeling (FDM), ink jet printing, 3-D printing, selective laser sintering, selective laser melting, 3-D laser cladding process, laminated object manufacturing and laser chemical capour deposition (Billiet et. al, 2012; Lan, 2009). It has been reported that RP can cut costs by up to 70 % and reduces time to market of finished parts by 90 % when compared to other conventional manufacturing methods (Lee et. al,

2014). A widely used technique of rapid prototyping involves FDM (McCullough and Yadavalli, 2013). In FDM, parts are fabricated by extruding a semi-molten polymer through a heated nozzle in a pre-scribed pattern onto a platform. The thermal energy associated with the semi-molten material drives the bonding and as the material is deposited, it bonds with the surrounding material, cools and solidifies (Singamneni et. al, 2012). Since the FDM process is one of the most important and widely used technologies. It has been closely studied with regard to the relationship between mechanical properties and process parameters (Galantucci et. al, 2010).

The porous scaffold architecture is important for new bone formation because the porous scaffold architecture can serve as a guiding substrate to enable the formation of a structural fibrous network as a pre-requirement for later bone formation (Nurizzati et. al, 2014). The importance of the three-dimensional (3-D) scaffold architecture for tissue engineering has been highlighted (Mekala et. al, 2013; Bagherzadeh et. al, 2014). A number of different processing techniques have been developed to design and fabricate 3-D scaffolds for tissue-engineering applications. The imperfection of the current techniques has encouraged the use of a RP technology known as FDM. A highly reproducible and computer-controlled method for designing and fabricating porous, bioresorbable 3-D scaffolds with FDM was developed (Jang et. al, 2013; Hutmacher et. al, 2001).

Surface modifications can change the topography or chemistry and sometimes even both the properties (Mishra and Kumar, 2014). Plasma based techniques furthermore offer several advantages when compared to other methods: plasma treatment is a dry and typically low temperature process, which limits the necessity to use solvents or potentially toxic substance and allows the processing of heat-sensitive materials (Chang and Chian, 2013). In addition, plasma processing of materials is very flexible and versatile and can be used for etching, texturing or chemical modification of surfaces as well as

for deposition of thin functional coatings (Multanen et. al, 2014). This modification can be done by changing the bulk properties of a material via chemical cross-linking of functional groups containing polymers or without changing the bulk properties via treatment with plasma polymers (Yang et. al, 2010). The plasma polymers are different from conventional polymers mainly because the conventional polymers are formed by well defined repeating units of monomers connected at regular intervals forming a polymer chain while plasma polymers form a cross-linked disordered network of the monomer units (Mishra and Kumar, 2014).

Bone morphogenetic proteins (BMPs) are the most important family of growth factors for bone regeneration and possess a wide array of biological activities, including cartilage induction, bone formation, organogenesis, cell differentiation, proliferation and apoptosis (Lin et. al, 2010). Fusion or self-assembly of BMP-2 mimetic peptide with other key domains have produced promising results presumably because two or more functional domains can control multiple or sequential cellular processes as required in bone tissue regeneration. In this respect, cell adhesive proteins such as Fibronectin and osteocalcin have been studied extensively and have been shown to preferentially bind to hydroxyapatite, as well as promote cell attachment, and osteogenic differentiation of progenitor cells (Marc A et. al, 2014). BMP-2 mimetic peptide, P24 has a very similar sequence to the 73-92 motif of BMP-2. thought to be a receptor-binding site on BMP-2 (Kazuhiro et. al, 2012). P24 is synthesized from the BMP native 73-92 amino acid region by adding 3 aspartic acids and one serine residue at the C and N termini of the peptide, respectively (Drevelle et. al, 2013). This peptide, covalently bound to or adsorbed onto materials such as PCL scaffolds can enhance the interaction of cells with the biomaterials (Niu et. al,2009). The P24 peptide was attached covalently to the functional group surface plasma polymerization to improve the adherence of osteoblast-like cells

(MC3T3-E1) to the modified substrates (Senta et. al, 2009).

In this study, BMP-2 mimetic peptide, P24 has already been clinically applied to accelerate bone regeneration in both fracture healing and spinal fusion. The sequence of P24, KIPKASSVPTELSAISTLYLDDD, is a part of the BMP binding site on BMP receptor 1Å. 3-D PCL scaffolds surface was functionalized with acrylic acid, allylamine, and DACH plasma polymerization and then immobilized with the P24 peptide to improve the biological behavior of preosteoblast cell. These results suggest that the P24 peptide immobilization in the 3-D PCL scaffolds has an effect on osteoblastic differentiation of MC3T3-E1 cells and can be used for the binding of bioactive molecules in bone tissue engineering.

Chapter 2. Background

1.1. Bone growth factors

Many growth factors, expressed during blood vessels development and induced angiogenic response to injury, are believed to play a significant role in the process of bone repair (Yancopoulos et. al, 1998; Noff et. al, 1989). These include members of the fibroblast growth factor, transforming growth factor, bone morphogenetic protein (BMP), Insulin-like growth factor, platelet derived growth factor, Vascular endothelial growth factor, hepatocyte growth factor, erythropoietin, growth hormone, as well as parathyroid hormone (Wang et. al, 2014).

Bone formation includes the coordination of multiple events such as activation, migration and differentiation of multiple cell types and tissues, which is regulated by a large number of growth factors. Biochemical stimulation of local bone healing through the delivery of growth factors supplement conventional bone repair therapies (Zouani et. al, 2013).

Bone repair can be modulated by different stimuli including growth factors. Transforming growth factor-β (TGF-β) is a cytokine known to be associated with the scarless healing of skin and it is highly probable that it may play a role in the repair of other tissue including bone (Sefat et. al, 2014). The TGF-β supergene family comprises several multifactorial gene products endowed with a vast pleiotropic activity regulating embryonic development, tissue patterning, postnatal tissue induction and morphogenesis, immunoregulation and fibrosis, initiating the morphogenesis of several tissue and organs including the skeleton and the bone matrix (Klar et. al, 2014).

1.2. Bone Morphogenetic Protein-2

BMP-2 was first isolated and identified from demineralized bone matrix by Marshall Urist in 1965s. Its extraction procedure was elaborate and laborious with poor recovery and the protein presented risks of immunological responses due to allogenic source. In late 1980s, molecular cloning was used to obtain recombinant human BMP-2 from eukaryotic expression systems like mammalian cells (Rane et. al, 2013). Recombinant growth factor delivery has been effective for a number of tissue engineering applications. In particular, BMPs which are potent osteoinductive growth factors, have been used extensively to treat bone defects in both research and clinical settings (Hettiaratchi et. al, 2014). As members of the TGF-β super family of growth factors, BMPs promote migration of many cells including osteoprogenitors and osteogenic differentiation of mesenchymal stem cells (Priddy et. al, 2014). However, they mediate a diverse array of developmental processes including cellular survival, proliferation, morphogenesis, cell fate commitment, differentiation and apoptosis (Tokola et. al, 2014). As the most representative bone groth factor, BMP-2 has been approved by the US FDA and the European Medicines Agency for the treatment of spinal fusion and tibial fractures combined with a matrix like collagen or decalcified bone (Wu et. al, 2014). BMP-2 induces bone formation by regulating the recruitment and differentiation of osteoprogenitor cells (Lu et. al, 2014). In addition, BMP-2 enhances the tendon-bone healing process and increases the biomechanical strength of tendon-bone junctions. However, BMP-2 has a short half life and is structurally unstable and thus requires a high dose administration, which can cause various adverse effects such as extensive ectopic ossification, immune reactions, soft-tissue swelling, seroma formation and paradoxical osteolysis (Kim et. al 2014).

1.3. BMP-2 mimetic peptide, P24

Though the recombinant DNA technologies allow sufficient supply of rhBMPs (recombinant human bone morphogenetic proteins) for research purpose, its heavy use in clinical practice is not only costly, but also associated with adverse effects such as overgrowth of bone and immune reactions. Recently it was reported that short peptide sequences of its core regions could mimic BMPs in terms of bone regeneration, suggesting that they can serve as an alternative inducer (Lin et. al, 2010). The peptide fragment is derived from the knuckle epitope of recombinant human BMP-2 protein (73-92) and binds BMP receptors I and II (Table 1). (Li et. al, 2010). *In vitro* experiments reveal that the synthetic peptide can precisely regulate biological behaviors of cells, such as adhesion and differentiation, via special cell communication. Meanwhile, it also owns excellent osteoinductivity and ectopic bone formation property *in vivo*, which is similar to those of BMP-2 (Niu et. al, 2009). The self-assembling peptides are special attractive platforms for engineering materials. Much research effort, has been focused on using short peptides to create a new generation of self-assembling scaffolds for use in biomedical applications recently. BMP-2 mimetic peptide, P24 has a very similar sequence to the 73-92 motif of BMP-2, thought to be a receptor-binding site on BMP-2. P24 is synthesized from the BMP native 73-92 amino acid region but adding 3 aspartic acids and one serine residue at the C and N termini of the peptide, respectively (Table 2). (Kazuhiro et. al, 2012).

Table 1. Function of P24 peptide (Duan et. al, 2007)

P24	**Template protein/source of peptide or sequence** **- Knuckle epitope/ 73-92 of BMP-2 (DDD were added)** **- KIPKASSVPTELSAISTLYLDDD**
	Function **- Regulate biological behavior of cells** **- Cells adhesion and differentiation**

Table 2. Anabolic functions and carriers of P24 peptide (Kazuhiro et. al, 2012)

P24	**Anabolic function and target** **- Yes** **- Ectopic bone formation** **- The target of BMP-related peptide, such as the BMP receptor on osteoblasts**
	Carrier **- PLGA-(PEG-ASP)** **- PLGA** **- Nano-HA/collagen/porus poly(lactic acid)(PLLA)** **- PLLA/chitosan microspheres (CM)**

PLGA : Poly (lactic-co-glycolic acid)

PEG : Poly (ethylene gilcol)

ASP : Aspartic acid

HA : Hydroxyapatite

Chapter 3. Materials and methods

1. Materials

1.1. Reagents and P24 peptide

PCL (melting temperature = 60 ℃, Mn = 45,000 g/mol) was purchased from Sigma-Aldrich. Acrylic acid (AAc, $C_3H_4O_2$, purity > 99%, Mw = 72.06) and 1,2-Diaminocyclohexane (DACH, $C_6H_{10}(NH_2)_2$, purity > 99%, Mw = 114.19) monomer were obtained from Sigma-Aldrich. Allylamine (AAm,CH_2:$CHCH_2NH_2$, purity > 97%, Mw = 57.09) monomer was obtained from Kanto Chemical. Toluidine blue O (TBO) and Methyl orange (MO) were purchased from TCI, tokyo chemical.

The synthetic BMP-2 mimetic peptide (P24) was produced from Lugen Sci Co., Ltd (Korea). The reagents and P24 peptide were used in this study as belows table 3.

Table 3. Detail analysis of peptide and HPLC

P24 peptide	
sequences	KIPKASSVPTELSAISTLYLDDD
purity (%)	94.48 (Fig. 1)
HPLC	
column (mm)	Kromasil (4.6*250) C18
wavelength (nm)	220
molecular weight	2463.79
Reagents and analysis	
26 and 51% acetonitrile	25 min
0.1% trifluoroacetic acid	mass spectrometer (Fig. 2)

HPLC (hight performance liquid chromatography)

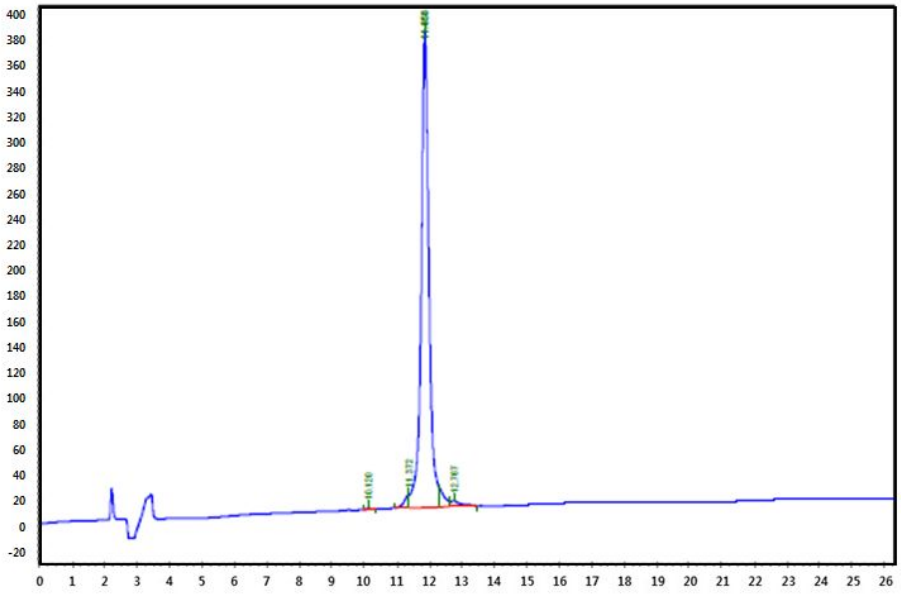

Fig. 1. The purity of P24 was 94.48% determined by HPLC.

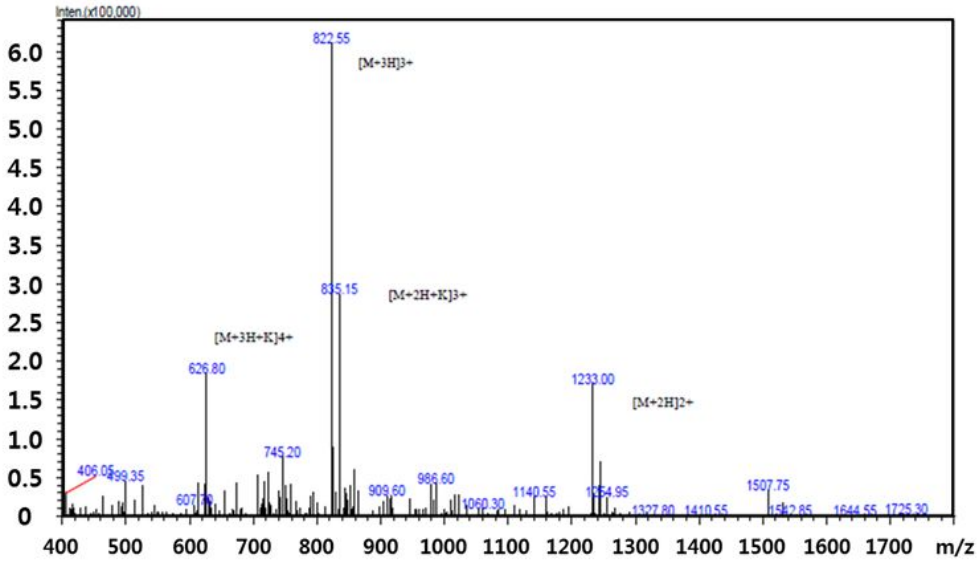

Fig. 2. Identify of the P24 was confirmed by analysis in a mass spectrometer.

2. Methods

2.1. Preparation of 3-D PCL scaffold and plasma-polymerization

2.1.1. Fabrication of 3-D PCL scaffolds

3-D PCL scaffolds were prepared by means of 3-D printing (3-D Bio Printer, M4T-100, M4T Co., Ltd, Korea). To obtain micro-sized struts of PCL scaffold, PCL pellet was injected into a heating cylinder at 90 ℃. The molten PCL was extruded through a heated 300 μm nozzle and compressed by pneumatic pressure of 580 ± 10 kPa.

Fig. 3 shows the Various patterns of 3-D PCL scaffold used in this study. The structure of 3-D PCL scaffold is compose of disc type with diameter 8 mm and height 1.5 mm. The strut of 3D PCL scaffolds could be plotted as layer-by-layer deposition at feed rate of 200 mm/min. And each layer was plotted using a layer thickness of 300 μm. PCL scaffolds were prepared with 0° / 45° architecture and pore size of approximately 150 μm.

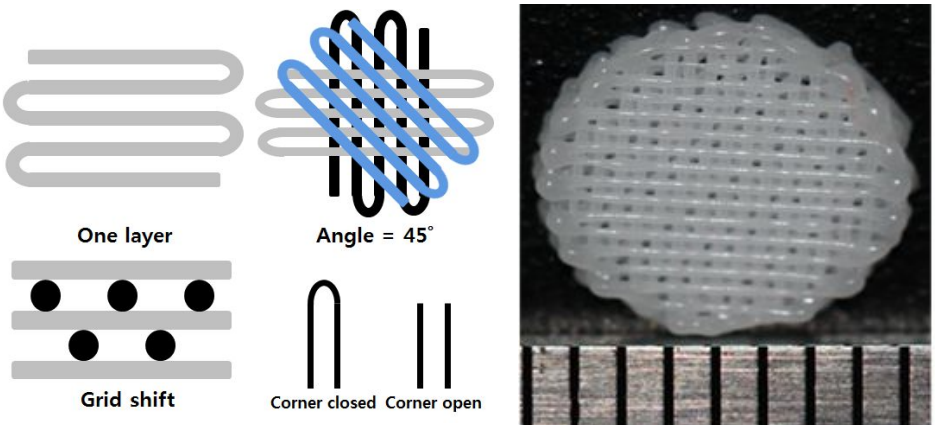

Fig. 3. Various patterns of 3-D PCL scaffold used in this study.

2.1.2. Acrylic acid, Allylamine, DACH plasma-polymerization

Plasma-polymerization was carried out a capacitively-coupled plasma reactor using a 13.56 MHz RF generator and matching network (mini plasma station, PLASMART, Korea) run in continuous wave mode (Fig.4),(Myung et. al, 2013). The samples were placed on a stage 3 cm away from the top electrode in the vacuum chamber. The plasma surface treatment is following as:

1) Acrylic acid plasma-polymerized (PPAAc) scaffolds were deposited at a RF power of 20 W, working pressure of 20 mTorr, and treatment time of 5 min.

2) Allylamine plasma-polymerized (PPAAm) scaffolds were deposited at a RF power of 100 W, working pressure of 100 mTorr, and treatment time of 5 min.

3) DACH plasma-polymerized (DACH) scaffolds were deposited at a RF power of 60 W, working pressure of 10 mTorr, and treatment time of 5 min.

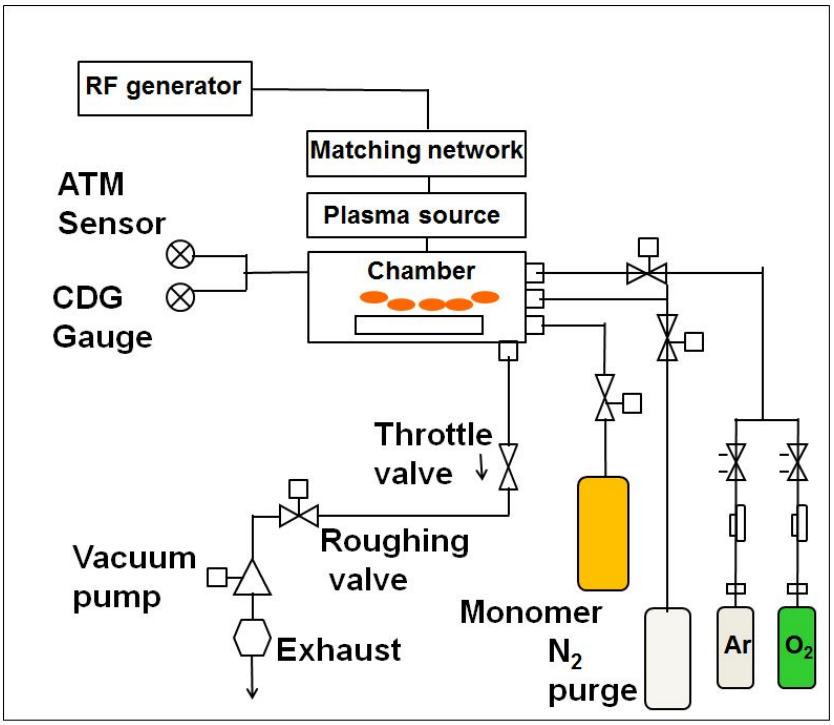

Fig. 4. Schematic diagram for plasma device.

2.1.3. Determination of carboxyl groups

The concentration of the carboxylic groups on the PCL scaffold surface after the acrylic acid grafting was determined by colorimetric titration method using TBO. TBO was diluted to a concentration of 500 μM in pH 10 water for binding to carboxyl functional groups. Sample surfaces were place in contact with the TBO solution for an hour. Subsequently, each sample was washed three times with water (adjusted to pH 10) to remove any unabsorbed dye. The dye was desorbed from the sample in a 50% acetic acid solution. Desorbed sample were measured for absorbance at a wavelength of 620 nm using a ELISA reader (G10S UV-Vis, Thermo Fisher SCIENTIFIC, China) (Kawashita et. al, 2003).

2.1.4. Determination of amino groups

MO is a negatively charged dye and can combine with positively charged amino groups on material surface under acidic condition by ion exchange mechanism (Zou et. al, 2014). The amino functionalized samples were treated with the acidic methyl orange solution (0.05% MO in a 0.1 M solution of sodium dihydrogen phosphate in water, filtered; pH app. 4.7) for 1 h. After rinsing the excess of dye with water, the sample were carefully pressed between tissue papers to remove the water. The fixed methyl orange was resolved by 5 mL of a 0.1 mL potassium carbonate solution and the concentration determined ELISA reader (G10S UV-Vis, Thermo Fisher SCIENTIFIC, China) at 465 nm. The $-NH_2$ content was obtained from a calibration plot of the optical density versus dye concentration with a 1:1 ratio assumed between the dye and amino groups.

2.2. Preparation of immobilized Peptide 3-D PCL scaffold

2.2.1. Immobilization of P24 peptide

The immobilization of the P24 peptide into the PCL modified surfaces was carried out through the 1-ethyl-3-(3-dimethylaminopropyl)carbodiimide (EDC, Sigma-Aldrich, USA), and N-hydroxysuccinimide (NHS, Sigma-Aldrich, USA) chemistry by the immersion of the samples into phosphate buffered saline (PBS, Welgene, Korea) solution containing 5 mg/mL of water-soluble EDC/NHS during 6 h at room temperature to activate the carboxyl groups at PCL surfaces (Puleo et. al, 2002). The concentration was EDC varied from 0.33 to 33 mM, and a 4:1 molar ratio of EDC to NHS was maintained. The peptide concentration was 800 μg/ml. Weakly bound peptide was removed from the samples by treatment with distilled water for three times. Samples were dried before use (Fig. 5).

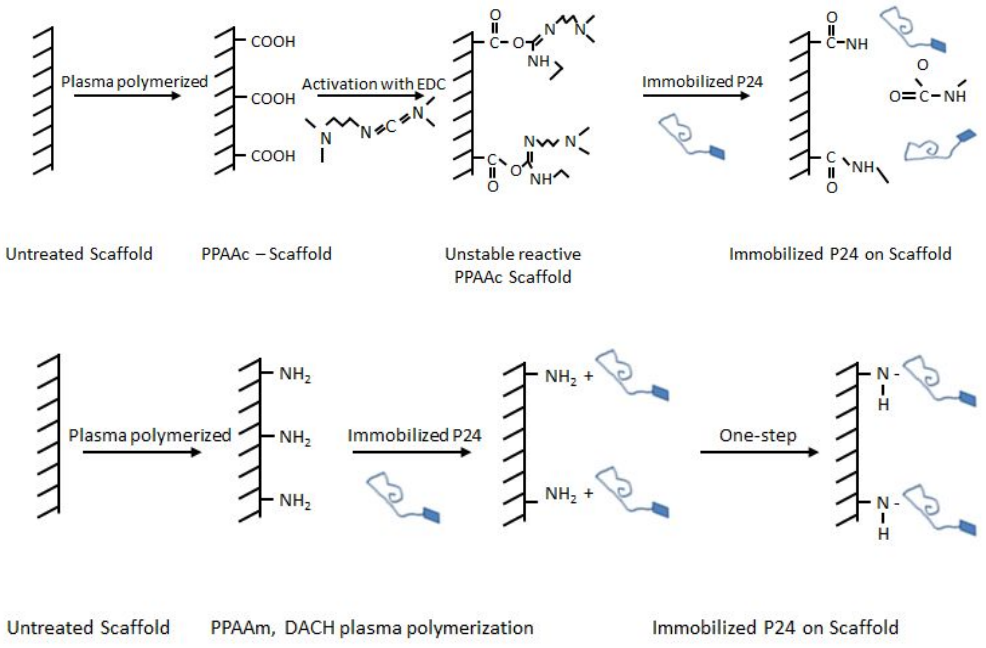

Fig. 5. Experimental scheme of overall immobilization process.

2.3. Surface characterization

2.3.1. Water contact angle analysis

To evaluate the general wettability of the surface, the contact angle was measured by the sessile drop method using a video contact angle instrument (water contact angle, GS, Surface Tech Co., Ltd, Korea) at room temperature. This measurements were used PCL films as sample. A smooth and uniform surface is a prerequisite for reliable contact angle determination. This was, however, impossible for microsphere scaffolds due to their size and shape. Thus, PCL films (0.5 ± 0.1 mm thickness and 20 mm diameter) were fabricated on glass slides. The contact angle was calculated as the angle between the PCL surfaces and the tangent of the liquid on the PCL surface using the Auto FAST algorithm and images analysis software.

2.3.2. FE-SEM analysis

The surface morphologies of pristine PCL scaffold and P24 peptide immobilized PCL scaffold were observed with a field emission scanning electron microscopy (FE-SEM, S-4800, Hitachi, Japan). Specimens were coated with Pt using a sputter-coater (ion-sputter, E1030, Hitachi, Japan). The accelerating voltage of FE-SEM images was 5 kV.

2.3.3. ATR-FTIR analysis

The chemical characteristics of pristine, plasma surface modified and P24 peptide immobilized PCL scaffolds were investigated by using attenuated total reflectance fourier transform infrared spectrometry (ATR-FTIR, Nicolet 6700, Thermo electron, USA). Every spectrum for samples was acquired in transmission mode with a resolution of 8 cm^{-1}, scan rate of 2 and spectral range of 4000-1500 cm^{-1}.

2.3.4. XPS analysis

The pristine, plasma surface modified and P24 immobilized on the PCL scaffolds were analyzed by X-ray photoelectron spectroscopy (XPS, VG Multilab 2000, ThermoVG Scientific, U.K). XPS measurements were performed by a spectrometer, samples for XPS analysis were 1.5 ± 1 mm thickness and 8 mm diameter. The X-ray source was monochromated aluminum, scanning over a binding-energy range of 0-1200 eV with a dwell time of 100 ms. The analyzer pass energy was 20 eV for C1s, N1s and O1s scans. Hight resolution spectra were obtained using a passing energy of 50 eV.

2.3.5. AFM analysis

Atomic force microscope (AFM, XE-100, Park systems, Korea) was used to measure the surface roughness of PCL scaffolds under non-contact mode with scan rate at 0.5 Hz, Z servo gain of 1. The silicon probe (PPP-NCHR, PointprobePlus, Nanosensors™, USA) has resonant frequency of 5 kHz. The scan area is 10 μm × 10 μm randomly selected from the scaffold surface. An arithmetic mean of the surface average roughness (R_a) was evaluated directly from the AFM images.

2.3.6. FITC-conjugation on PCL films

The P24 peptide immobilized PCL films were immersed in the FITC-labeled P24 solution (FITC-P24 800 μg/mL) for 30 min in room temperature respectively. The same samples were reported already like 2.3.1. FITC is a fluorescein molecule functionalized with an isothiocyanate reactive group (-N=C=S) at one of two hydrogen atoms on the bottom ring of the structure. This derivative is reactive towards the primary amine groups on proteins, peptides and other biomolecules. The labeling reaction was initiated by adding a P24/PBS solution (1 mg/mL) to a FITC/PBS solution (0.2 mg/mL). The mixtures were kept in the dark at 0-4 ℃ overnight according to the literature (Seo et. al, 2010). FITC allows direct visualization of the immobilized peptide using fluorescent microscopy.

2.4. *In vitro* bioactivity in osteoblast cell

2.4.1. Culture of MC3T3-E1 cells

Pre-osteoblast cells from the cell line MC3T3-E1 (calvaria newborn mouse derived, ATCC, CRL-2953) were cultured in α-minimum essential medium (Gibco, USA) supplemented with 10% fetal bovine serum and 1% penicillin-streptomycin, and kept at 37 ℃ in a saturated humid atmosphere containing 95% air and 5% CO_2. The cells were detached with a trypsin-EDTA solution (Sigma-Aldrich, USA) and suspended in the medium. Before cell seeding, the samples were placed in 48-well culture plates and sterilized by soaking the samples in 70% ethanol for 15 min. The cells were seeded on sterilized samples at a cell seeding density of 1×10^5 cells/mL.

2.4.2. MTT assay

A MTT, a water-soluble yellow dye that can be reduced to water-insoluble purple formazan crystals by the dehydrogenase system of active cells, assay was used to examine the level of cell attachment and proliferation, as described elsewhere. Selected PCL scaffolds were immersed in the culture medium and sterilized by exposure under an ultraviolet (UV) lamp for 1 day. Then the scaffolds were transferred to new 48-well plate. The cultured MC3T3-E1 cells and the culture medium (1.0 mL/well) were seeded and added to each well (cell density, 1×10^5 cells/specimen) to reach a level above that of the scaffolds. The target point (1, 4 and 6 days), the cells were rinsed with PBS of 1 mL and incubation (5%/CO_2) with 100 μL of the MTT solution (Sigma-aldrich, USA) per well at 37 ℃ for 4 hours. The MTT solution was made by dissolving to a concentration of 0.5 g/L in sterilized PBS. After 4 hours of incubation at 37 ℃, the solution was removed, 1 mL of dimethyl sulfoxide (DMSO, JUNSEI) was added and after 10 min of slow shaking, a 200 μL aliquot of the solution from each well was aspirated and poured onto a 96-well plate to measure the absorbance at 540 nm using an EPOCH, absorbance microplate reader (BioTek Instruments Inc, USA).

2.4.3. Alkaline phosphatase (ALP) activity assay

The level of osteogenic differentiation induced by the ALP activity of the MC3T3-E1 cells plated at 1 × 10^5 cells/well in 48-well plates at 7 and 14 days on each specimen (PCL, PCL/PPAAc, PCL/PPAAm, PCL/DACH, PCL/PPAAc/P24, PCL/PPAAm/P24 and PCL/DACH/P24) were assayed using a standard ALP test procedure. The cells were rinsed with PBS. The ALP activity in the cell lysate was determined by measuring the level of *p*-nitrophenol (*p*-NP) released from disodium *p*-nitrophenyl phosphate (*p*-NPP). The cells were lysed by adding a lysis buffer for 20 min. The lysis buffer was prepared by mixing 0.2% Triton-X-100, 0.9% NaCl in distilled water. 150 μL of the cell lysate was collected, centrifuged at 3000 rpm for 10 min at 4 ℃, and placed on ice. The supernatant was transferred into a eppendorf tube for determining the alkaline phosphate assay and protein concentration. For the ALP assay, an ALP test premixture (100 μL of cell lysate solution, 200 μL of 0.1 N glycine-NaOH buffer, 100 μL of 15 mM *p*-NPP and 200 μL of D.W) was added to each tube and incubated at 37 ℃ for 30 min. After adding 600 μL of 1.2 N NaOH to the tubes, the absorbance was measured by EPOCH, absorbance microplate reader (BioTek Instruments Inc, USA) at 405 nm. The protein concentration of the cell lysate was determined by BSA method (BSA protein assay kit, pierce, Rackford, IL, USA) according to the manufacture's protocol. The ALP activities were normalized by the protein content of the cell lysate and expressed in *p* mol *p*-NP/min/μg protein.

2.4.4. SEM analysis

The morphology of PCL scaffold before the culturing and after 30 min of culture was examined. Previously the samples seeded with cells were carefully washed with DPBS and fixed in 2.5% glutaraldehyde (Sigma-aldrich, USA) solution at 4 ℃ for 3 hours. The samples were dehydrated in a graded series of aqueous ethanol solutions (70%, 90%, 95%, 100%) for 5 min each and then placed in hexa-methyl-di-silazane solution (Fulka) to remove any alcohol. After 10 min, the solution were removed and the scaffolds were allowed to air dry overnight at room temperature. All dried samples were sputter coated with gold and examined by scanning electron microscopy (SEM, SNE-3200M, SEC Inc., Korea) at a voltage of 15 kV.

2.4.5. Fluorescence images

Cell viability was determined by staining cells using a live/dead viability/cytotoxicity kit(Biovision). The LDS procedure the double-staining of cells with propidium iodide, a fluorescent-red dye that stains membrane compromised cells (dead cells), a fluorescent-blue dye that stains all cells (live cells). In brief, MC3T3-E1 cells were seeded at a density of 1×10^5 cells/mL on the surface of a series of PCL scaffolds in 48-well plates. After a 48 h incubation, cells/specimens were rinsed three times with DPBS (Welgene, Korea) and then incubated with LDS solution (1 mM Live Dye and 2.5 mg/mL of Propidium iodide of 0.25 mL per well was added and culture plates were returned) for 20 min at room temperature. Viable cells (green) and dead cells (red) were counted under a fluorescent (NI-SS, Nikon, Japan).

MC3T3-E1 cells cultured on PCL scaffolds for one day were washed in DPBS, fixed with freshly prepared 4% paraformaldehyde (Electron Microscopy Science) for 30 min. Fixed cells were washed with DPBS, followed by permeabilization with 0.1% Triton X-100 buffer (Sigma-aldrich, USA). After 5 min of incubation with a blocking buffer containing 1% bovine serum albumin (1% BSA, 1X PBS), cells were incubated for 15 min with Rhodamine-phalloidin (Molecular probes, life-technologies, India) diluted 1:100 in PBS. PCL scaffolds were washed three times with DPBS, mounted on cover glass for mociscopy with fluorescence mounting media DAPI (Vector Laboratories Inc., USA) DAPI was used as a counterstain for the nucleus. Samples were inspected by fluorescent microscopy (NI-SS, Nikon, Japan)

2.4.6. Bone mineralisation

Calcification deposits on cells were quantified as described by Girish et. al, 2011. At the differentiation days of 7 and 14 days, cells were washed with PBS twice and then fixed with 2.0% formaldehyde. The cells were stained with 40 mmol/L of alizarin red S solution (pH 4.4) for 40 minutes at room temperature and rinsed with deionized water twice. The images of stained cells were captured using a digital camera (Cho et. al, 2010).

2.4.7. Statistical analysis

Student's *t*-test as used for all statistical analyses. $P < 0.05$ and $P < 0.01$ were considered statistically significant.

Chapter 4. Results and discussion

1.1. Surface characterization

Fig. 6. shows the Photograph images of carboxyl and amino density; this images changed with the plasma-polymerized monomer. Fig. 7. shows the change of carboxyl groups density as a function of the RF power applied. The carboxylic density of the PPAAc thin film decreased with increasing input power. From this result, it was found that optimum condition of acrylic acid plasma-polymerization is 20 W of RF power. Since then, PPAAc scaffolds were treated with this condition. The -COOH density was also evaluated with TBO test. These data are expressed as "apparent" surface density. After 100 W the density reached a maximum decreased. (Detomaso et. al, 2005).

Mo test was investigated on $-NH_2$ coated (PPAAm and DACH) at different RF power values. Fig. 8 and 9 show the effect of the RF input power on the scaffold surface density of the amino groups were found to increase as a function of the RF power applied. The hydrophilicity is influenced by hight $-NH_2$ grafted density on the modified surface, optimized plasma-polymerization process (power input 100 and 60 W) and treated all plasma-polymerized samples (PCL/PPAAm and PCL/DACH) with this conditions. The higher nitrogen content incorporated in DACH than that of allylamine under the same experimental conditions was also observed in literature (Mangindaan et al, 2011).

Fig. 10. shows the contact angle values of hydrophilicity of the unmodified and modified PCL film surfaces, were measured. The water contact angle of pristine PCL film was 54.46° . With the introduction of DACH onto the film surface, the water contact angles dropped to 36.56° . With the

introduction of PPAAm onto the film surface, the water contact angles dropped to 37.57° . With the introduction of PPAAc onto the film surface, the water contact angles dropped to 27.23° . The water contact angle decreased after the each plasma polymerized. Although the surface of DACH and allylamine have very low contact angle similar to the Acrylic acid surface, both surfaces must be modified differently with the surface of carboxyl and amine functional group, respectively. This reveals that three types of plasma polymerized scaffolds were not hydrophobic materials (Cheng and Teoh, 2004). Therefore, The cells adhered at higher numbers to more hydrophilic materials and spread over a larger area (Myung et. al, 2013).

3-D PCL scaffold morphology and peptide constructs was studied using FE-SEM (Fig. 11). Pristine PCL scaffold (a), surface modified scaffold (b), and P24 immobilized scaffold (c and d). After peptide immobilizing, surface topography became changed while the interconnected pore structure remained the same in all scaffolds (Kong et. al, 2014). The peptide molecules occupied ~10~20% surface area of the total surface area of the scaffold (Sousa et. al, 2014).

Fig. 12. shows the respective ATR-FTIR spectra of pristine PCL scaffold (a), PCL/PPAAc (b), PCL/PPAAm (c), PCL/DACH (d), PCL/PPAAc/P24 (b-1), PCL/PPAAm/P24 (c-1) and PCL/DACH/P24 (d-1) scaffold. In the PCL spectrum, a major absorption peak appeared at 1712 cm^{-1} according to the functional group, C=O, in PCL scaffold (Gupta B et. al, 2002). The same peak was also found in the spectrum of all groups. A new peak at 2358 cm^{-1} that was attributed to the absorption of P24 groups appeared. PCL/P24 groups spectra demonstrate the successful immobilization of the peptide: the Amide I absorption (ν C=O) in the region between 1639 and 1682 cm^{-1}, and the Amide II absorption (δ N-H) between 1528 and 1567 cm^{-1} can be observed

(Sartori et. al, 2008). The differences observed in terms of the absorbance between the peptide spectra's can be related with the surface modification between the samples (Qu et. al, 2007).

Fig. 13. the XPS wide scan spectrum of the pristine PCL surface is showed in (a). It reveals that oxygen and carbon signals are present. The spectrum of PCL/PPAAc scaffold surface (b) also shows the same peaks as pristine PCL surface corresponding to N1s. However, the relative intensity of oxygen and carbon peaks varied after grafting with acrylic acid. In contrast, a new peak corresponding N1s appeared on the spectrum of PCL/PPAAm, PCL/DACH, PCL/PPAAm/P24, PCL/DACH/P24 and PCL/PPAAc/P24 scaffold surfaces (c, d, c-1, d-1 and b-1) (Lee et. al, 2013).

Fig. 14. shows the respective C1s core-level spectra of the (a) PPAAc group, (b) allylamine group and (c) DACH group scaffold surfaces. In the case of (a), (b), (c) and (d) scaffold surfaces, the C1s core level spectrum contains four major peak components, with binding energy at 284.7 eV for the C-H species, at 286.6 eV for the C-O species and at 288.8 eV C=O species. After P24 immobilization onto the scaffold surface, the C1s core level can be curve-fitted with four peak components, with binding energy at 282.6 eV C-N species, at 284.2 eV C-NH species, at 287.6 eV N-C=Oespecies and at 285.8 eV C-O, C=N, -C=N species (Lee et. al, 2008).

Fig. 15. shows the AFM images of pristine PCL scaffold (a), PCL/PPAAc scaffold (b), PCL/PPAAm scaffold (c), PCL/DACH scaffold (d), PCL/PPAAC/P24 scaffold (b-1), PCL/PPAAm/P24 scaffold (c-1) and PCL/DACH/P24 scaffold (d-1). The (a) scaffold had a roughness of 6.961 nm and (b), (c) and (d) scaffold had a roughness of 8.361 nm, 7.800 nm and 8.090 nm respectively. Also show the (b-1), (c-1) and (d-1) scaffold had a roughness of 10.401 nm,

13.825 nm and 15.117 nm respectively. The surface topography of scaffold undergoes significantly changes as a result of the plasma treatment and peptide immobilization process. This could be due to the mechanism of the surface modification, which is initiated by radicals generated at the scaffold surface (Cheng and Teoh, 2004). These radicals initiated the surface modification of the DACH, allylamine and acrylic acid. PolyDACH, polyallylamine and polyacrylic acid grafted on the surface has a thickness in sub-micron range (Cai et. al, 2013). As a result, the roughness of the (b), (c) and (d) scaffold surface increased in comparison with the pristine PCL scaffold. P24 was immobilized via the covalent bond with each poly monomer by losing a water molecule. P24 immobilization broadened the each poly monomer domains on the scaffold surface, which led to increase of the roughness of the surface.

Fig. 16. shows the FITC images of pristine PCL (a), PCL/PPAAc/P24 scaffold (b), PCL/PPAAm/P24 scaffold (c) and PCL/DACH/P24 scaffold (d). The fluorescence micrograph (Fig. 19) clearly shows green fluorescence spots distributed over the PCL scaffold surfaces, which shows that the bio-active P24 peptide had been immobilized successfully on the surface. However, no fluorescence probe could be detected in the unmodified PCL scaffolds (Zhao et. al, 2005).

1.2. *In vitro* bioactivity in osteoblast cell

P24 is responsible for generating appropriate biomimetic environment for enhanced viable cell attachment, cell bonding and the initiation of a cascade of events (migration, alignment, proliferation and differentiation) that are necessary for optimal bone formation (Hanks and Atkinson, 2004).

Fig. 17. shows the numbers of viable cells on the PCL scaffolds at 1, 4 and 6 days of culture as determined by MTT assay. The cells proliferated on all PCL scaffolds during the culture period. The cell proliferation rate of the control and all experimental groups increased with culture time. After 6 days cell viability was significantly higher on the modified PCL scaffolds and P24 immobilized PCL scaffolds of DACH groups than the pristine PCL scaffolds. DACH-NH_2 contains nitrogen-containing groups at relatively high concentration, which are well known to play pivotal roles in cell adhesion and proliferation. It was also indicated that amino groups are favorable for the immobilization of adhesive cell proteins (Ko et. al, 2013).

Fig. 18. shows the ALP activity of MC3T3-E1 cells grown on the PCL scaffolds for 7 and 14 days. The normalised OD value of the PCL scaffold was set as 100% and the values of the modified scaffolds were compared. At 7 days, ALP activity was not different between the scaffolds, but at 14 days a significant difference was evident. Additionally, the PCL/DACH/P24 scaffolds showed the highest ALP levels after 14 days of culture. Based on the results of ALP activity deposition, suggest that the PCL/DACH/P24 group scaffolds provided better micro-environmental biological conditions for the pre-osteoblast cells than the pristine PCL scaffold (Puleo et. al, 2002).

Cell morphology and cellular on 3-D PCL scaffold constructs, was studied using SEM (Fig. 19). The cell morphologies showed that the attached cells exhibited a good spreading appearance on the modified PCL scaffold as compared to that on the untreated PCL scaffold (Serrano et. al, 2014). It was observed that PCL/DACH/P24 showed enhanced cell-binding capacity due to its biomimetic nature which resulted in significantly higher viable cell attachment in comparison to PCL/PPAAc/P24 and PCL/PPAAm/P24 scaffold.

In this work, viability and proliferation of cells in the scaffolds were evaluated combining live and dead cells, rhodamine-phalloidin. Fig. 20 fluorescence displays green and red indicate live and dead cells, respectively. The pristine PCL scaffold did not support cell growth well, presumably due to the hydrophobic properties of PCL (Veleirinho et. al, 2013). PCL/DACH/P24 showed significantly higher cell viability efficiency than PCL/PPAAc/P24 and PCL/PPAAm/P24. This may be attributed to the ability of DACH plasma surface modification to enhance cell viability.

The morphology of the adhered osteoblastic cells on the 3-D PCL scaffolds is shown in the confocal fluorescence microscopy images of (Fig. 21), depicting the stained nucleic acid in the cell nuclei in purple, the actin cytoskeleton in red. The PCL/DACH/P24 scaffolds showed higher numbers of nuclei and a well-developed actin cytoskeleton than the other scaffolds. This may be due to provision by the P24 peptide of a more attractive microenvironment for the seeded cells, because the than the other scaffold immobilized with peptides such as the P24 peptide (Kim and Kim, 2014).

Fig. 22. shows alizarin red S images of the 3-D PCL scaffolds. In the presence of peptide, significant alizarin red staining was apparent in plasma-polymerized groups. A hight intensity of alizarin red (red

colouration) staining indicates a higher calcium concentration. The highest mineralisation was found in the PCL/DACH/P24 scaffold in 14 days (Lee et. al, 2014). The formation of a peptide matrix with mineralization is a prerequisite for a good bone formation process as mineralization plays a role in dictating and spatially orienting the deposition of extracellular matrix (Verma and Kumar, 2010).

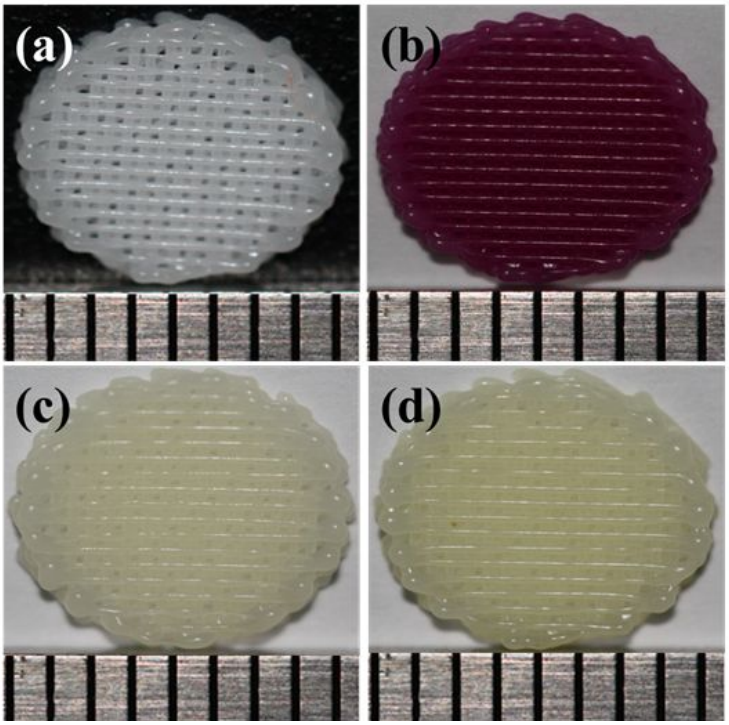

Fig. 6. Photographs of the PCL scaffold treated TBO (carboxyl) and MO (amine) after plasma-polymerized. (a) pristine PCL scaffold, (b) PPAAc-PCL scaffold , (c) PPAAm-PCL scaffold, and (d) DACH-PCL scaffold.

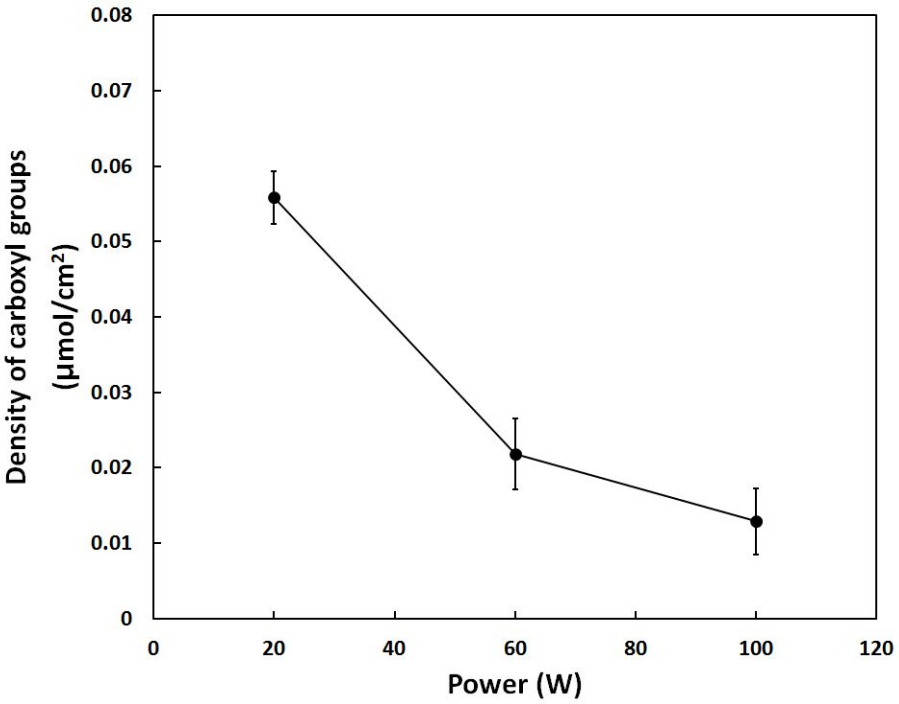

Fig. 7. Surface concentration of -COOH groups versus RF power.

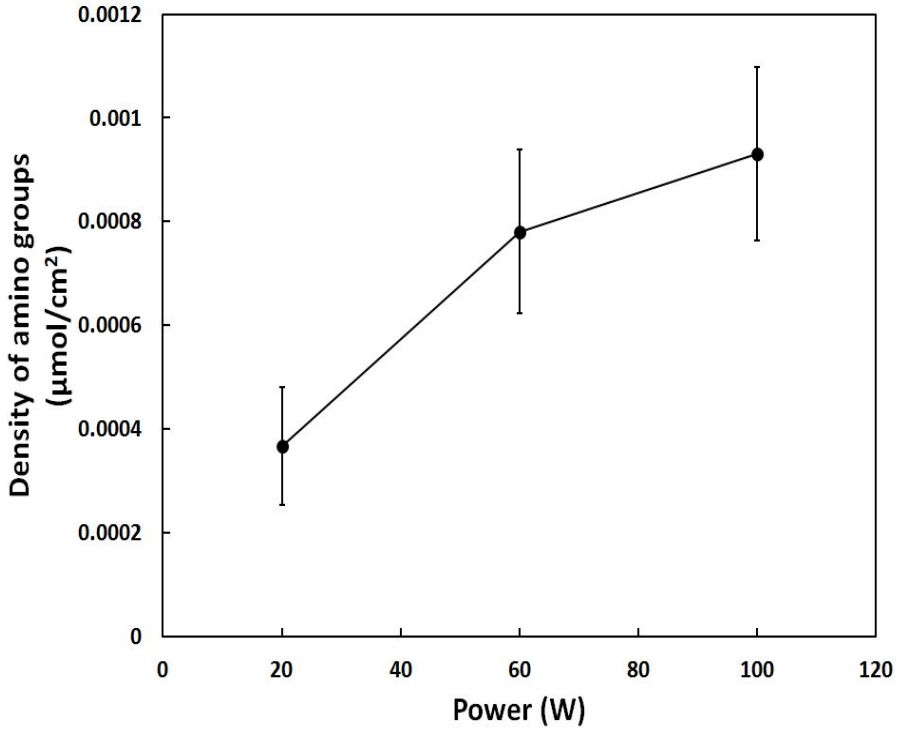

Fig. 8. Surface concentration of $-NH_2$ (allylamine) groups versus RF power.

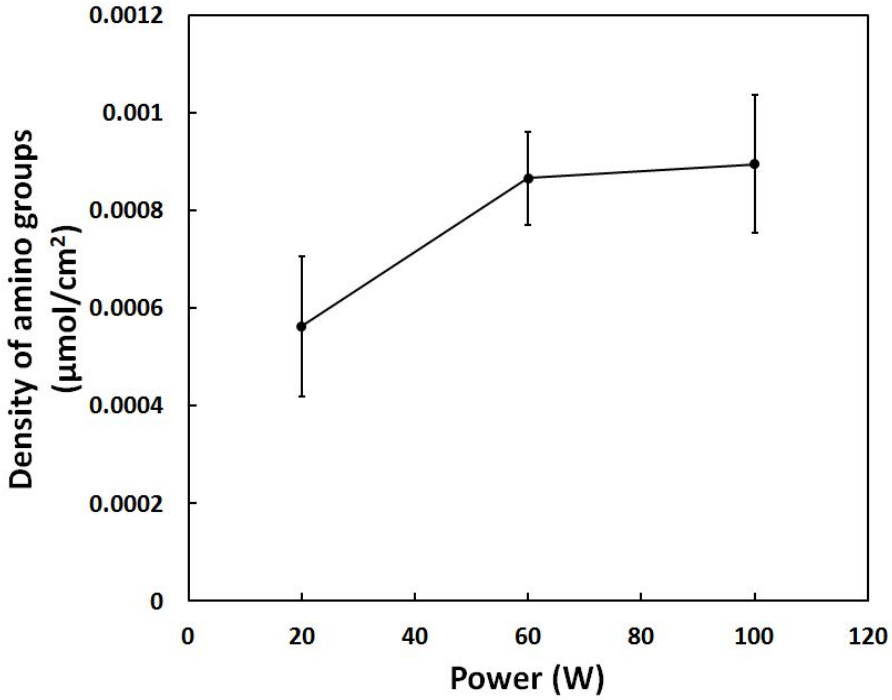

Fig. 9. Surface concentration of $-NH_2$ (DACH) groups versus RF power.

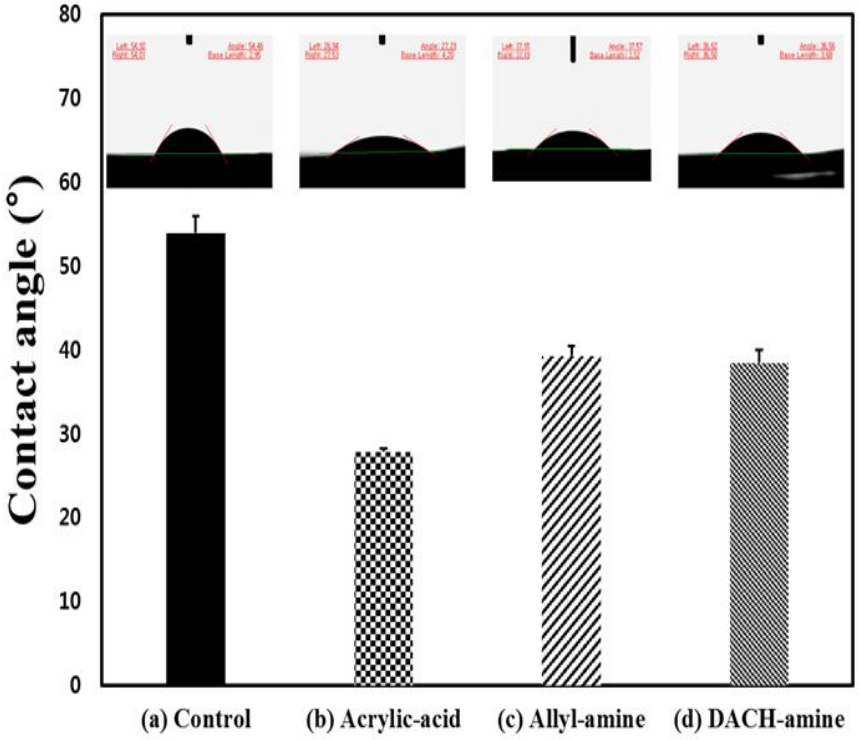

Fig. 10. Contact angles of (a) pristine PCL surface, (b) PCL/PPAAc surface, (c) PCL/PPAAm surface, and (d) PCL/DACH surface.

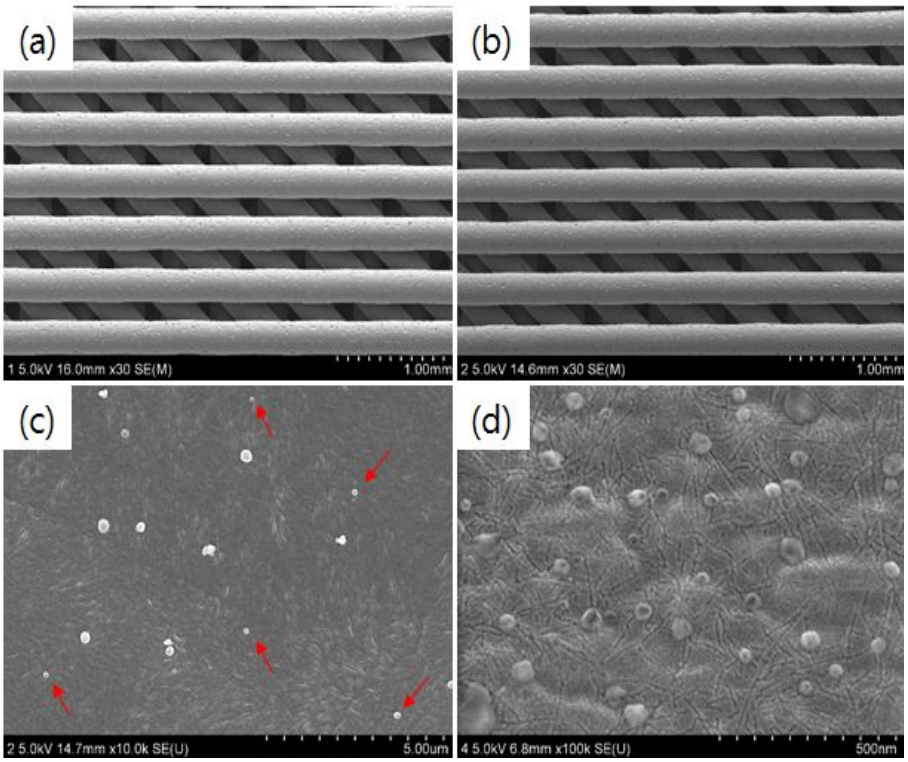

Fig. 11. FE-SEM images of (a) pristine scaffold, (b) surface modification scaffold, and (c and d) immobilized peptide scaffolds.

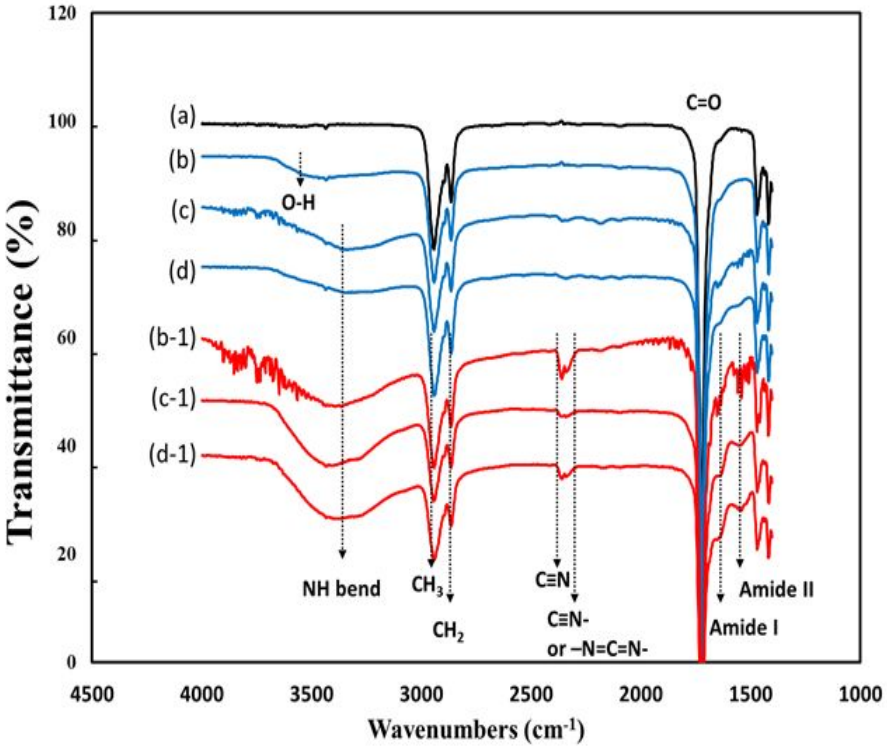

Fig. 12. ATR-FTIR analysis of (a) pristine PCL surface, (b) PCL/PPAAc surface, (c) PCL/PPAAm surface, (d) PCL/DACH surface, (b-1) PCL/PPAAc/P24 surface, (c-1) PCL/PPAAm/P24 surface, and (d-1) PCL/DACH/P24 surface.

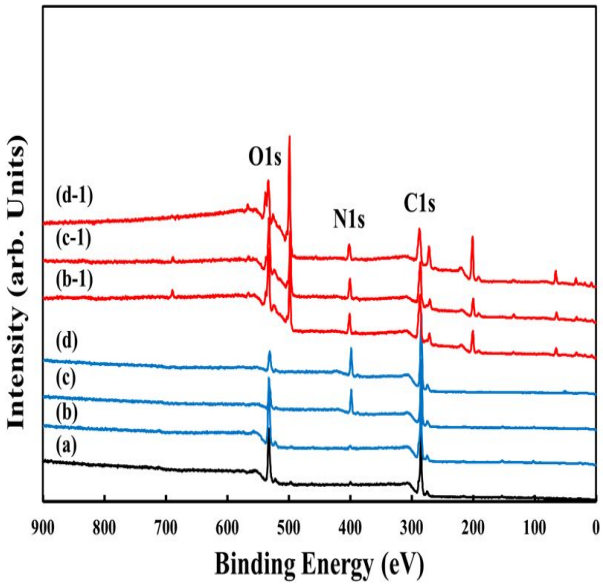

	% C	% O	% N	O/C ratio	N/C Ratio
Control	74.48	23.43	1.69	0.31	0.02
PPAAc	73.41	25.32	1.27	0.34	0.01
PPAAm	76.05	10.53	13.42	0.13	0.18
DACH	77.57	8.54	13.89	0.11	0.18
PPAAc-P24	63.5	26.06	10.44	0.41	0.16
PPAAm-P24	61.87	26.76	11.37	0.43	0.18
DACH-P24	58.52	30.49	10.99	0.52	0.19

Fig. 13. XPS wide scan spectra of (a) pristine PCL scaffold, (b) PCL/PPAAc scaffold, (c) PCL/PPAAm scaffold, (d) PCL/DACH scaffold, (b-1) PCL/PPAAc/P24 scaffold, (c-1) PCL/PPAAm/P24 scaffold, and (d-1) PCL/DACH/P24 scaffold.

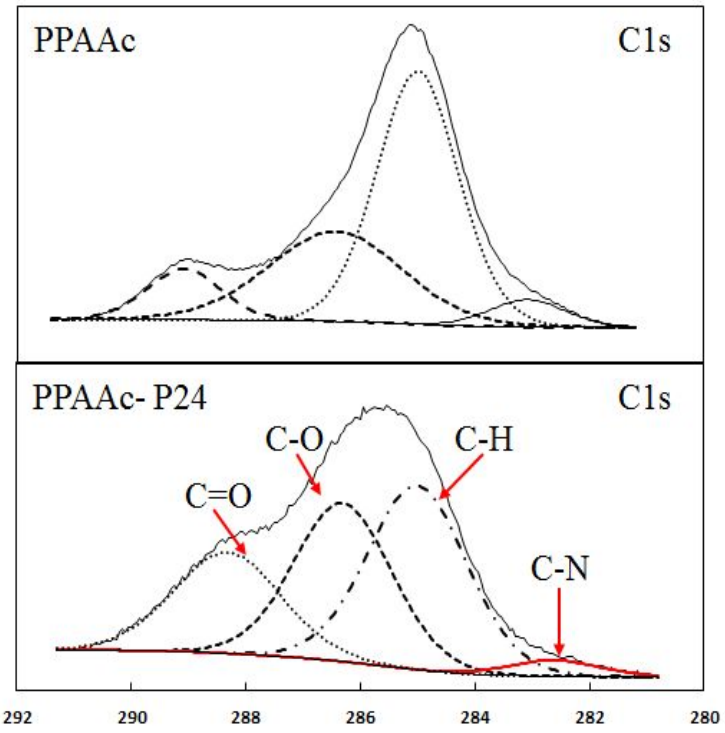

Fig. 14(a). Surface chemical composition of the PCL/PPAAc scaffolds examined by XPS. High-resolution C1s peaks.

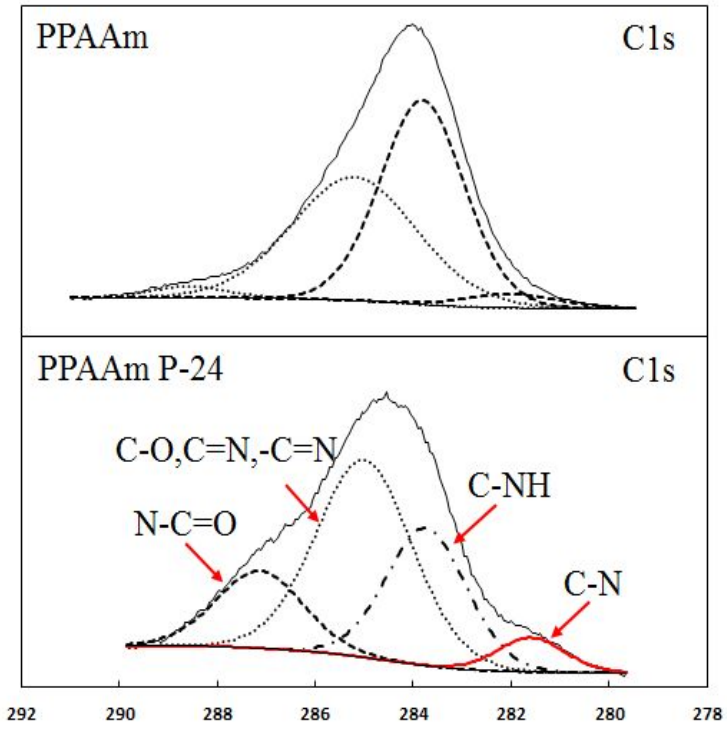

Fig. 14(b). Surface chemical composition of the PCL/PPAAm scaffolds examined by XPS. High-resolution C1s peaks.

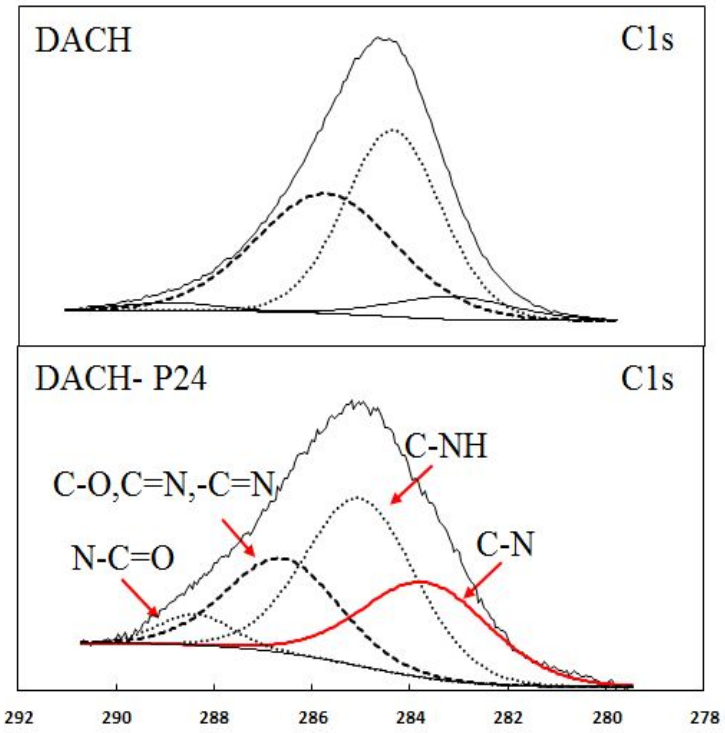

Fig. 14(c). Surface chemical composition of the PCL/DACH scaffolds examined by XPS. High-resolution C1s peaks.

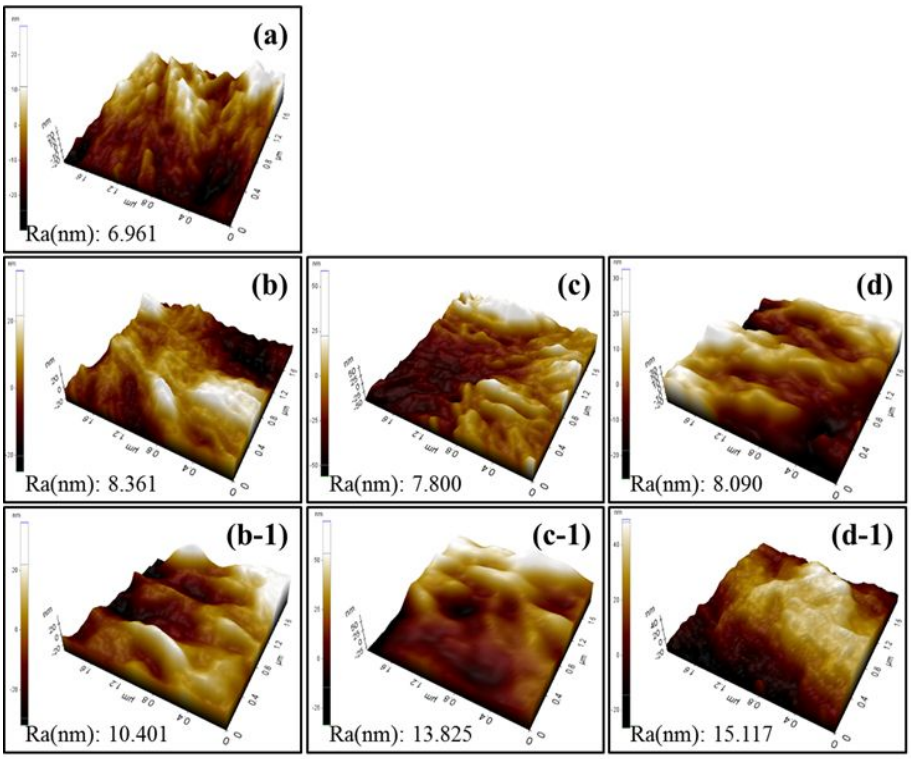

Fig. 15. AFM images of (a) 1.99 μm × 1.99 μm pristine PCL scaffold, (b) PCL/PPAAc scaffold, (c) PCL/PPAAm scaffold, (d) PCL/DACH scaffold, (b-1) PCL/PPAAc/P24 scaffold, (c-1) PCL/PPAAm/P24 scaffold, and (d-1) PCL/DACH/P24 scaffold.

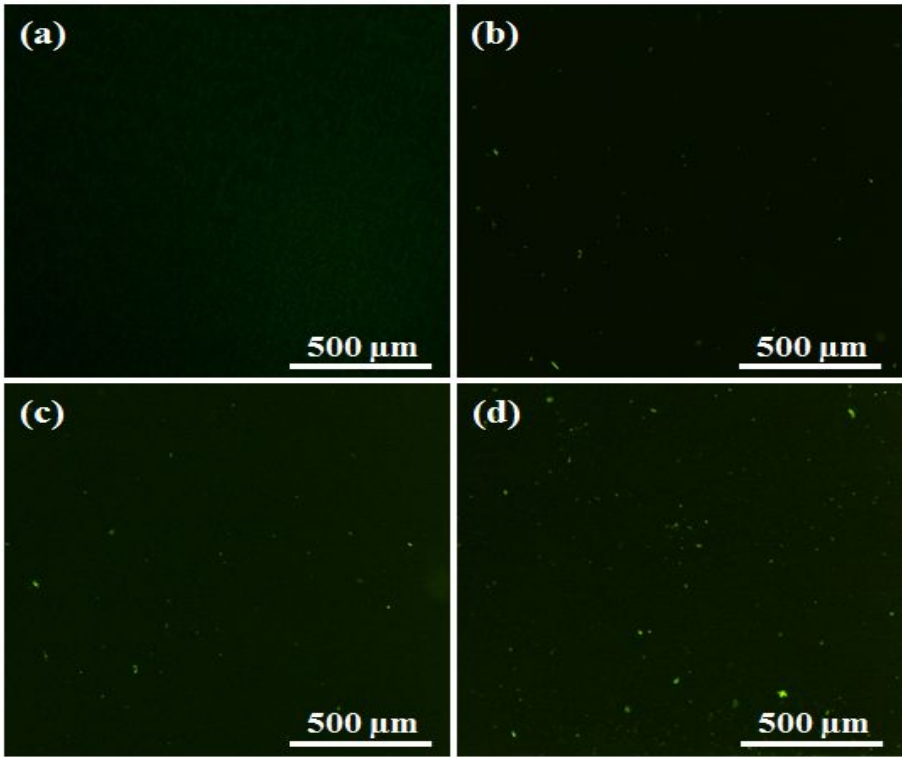

Fig. 16. Fluorescence microscopy images of FITC labeled P24 peptide immobilization on the control (a), PCL/PPAAc (b), PCL/PPAAm (c), and PCL/DACH (d) surfaces.

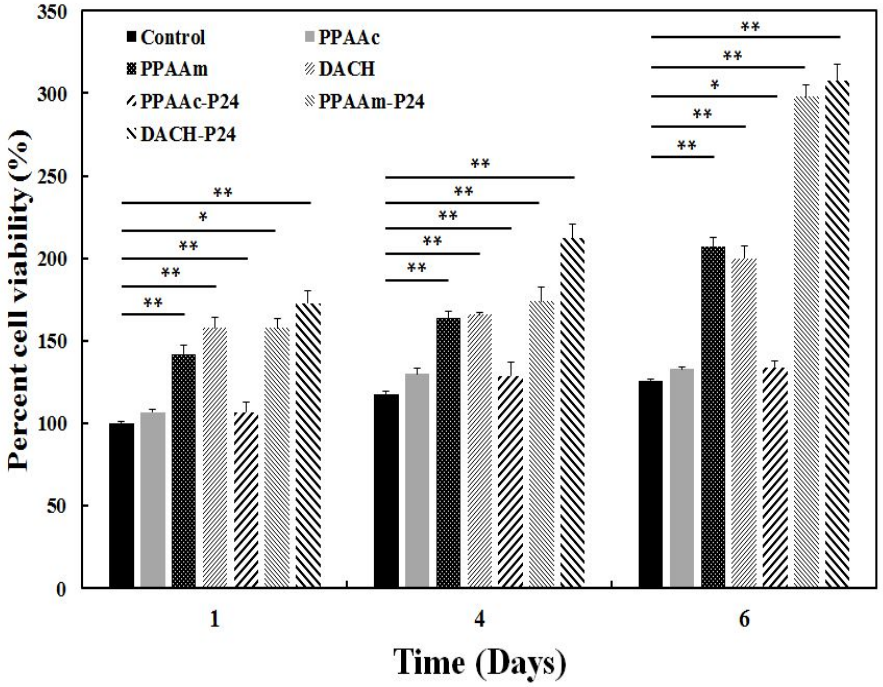

Fig. 17. The proliferation of MC3T3-E1 cells cultured on the various 3-D PCL scaffolds for 1, 4, and 6 days.

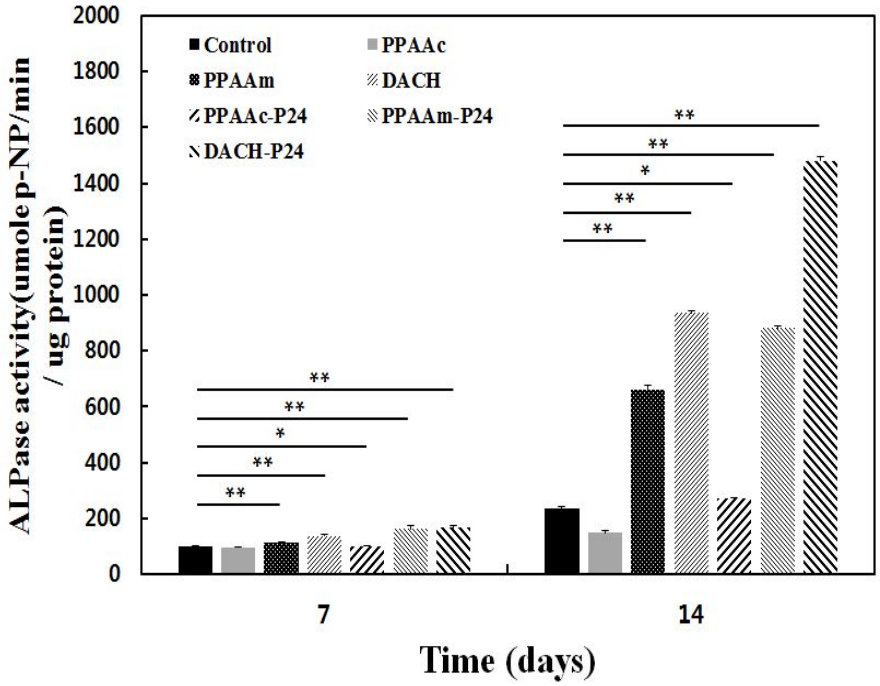

Fig. 18. The ALP activity of MC3T3-E1 cells cultured on the various 3-D PCL scaffolds for 7 and 14 days.

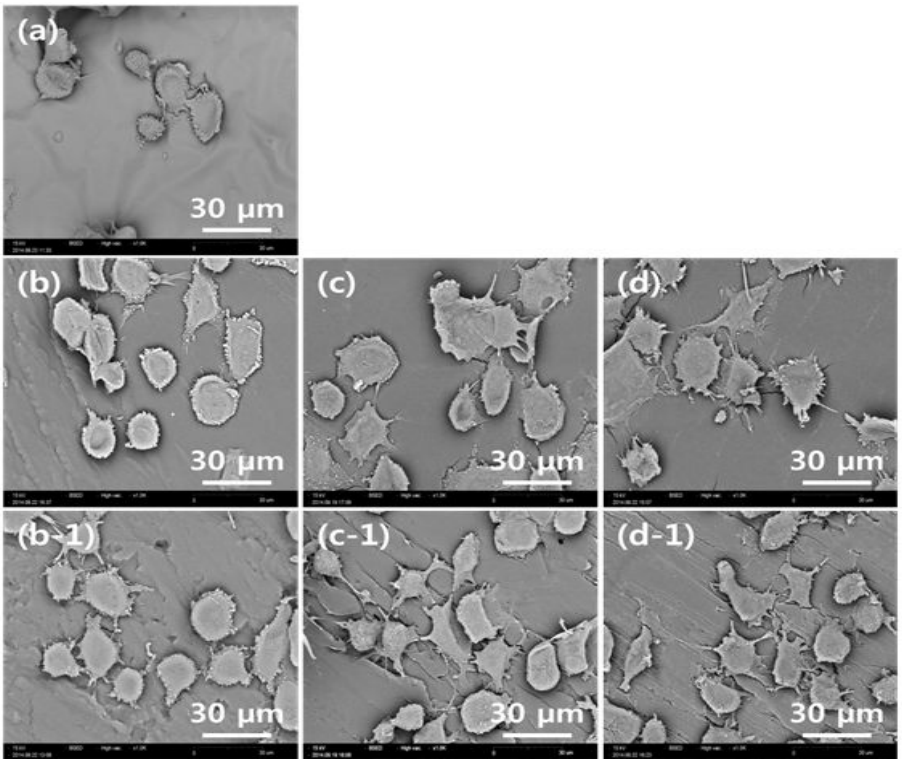

Fig. 19. SEM images of MC3T3-E1 on the (a) pristine PCL scaffold, (b) PCL/PPAAc scaffold, (c) PCL/PPAAm scaffold, (d) PCL/DACH scaffold, (b-1) PCL/PPAAc/P24 scaffold, (c-1) PCL/PPAAm/P24 scaffold, and (d-1) PCL/DACH/P24 scaffolds after 30 min of cell incubation. (×1000)

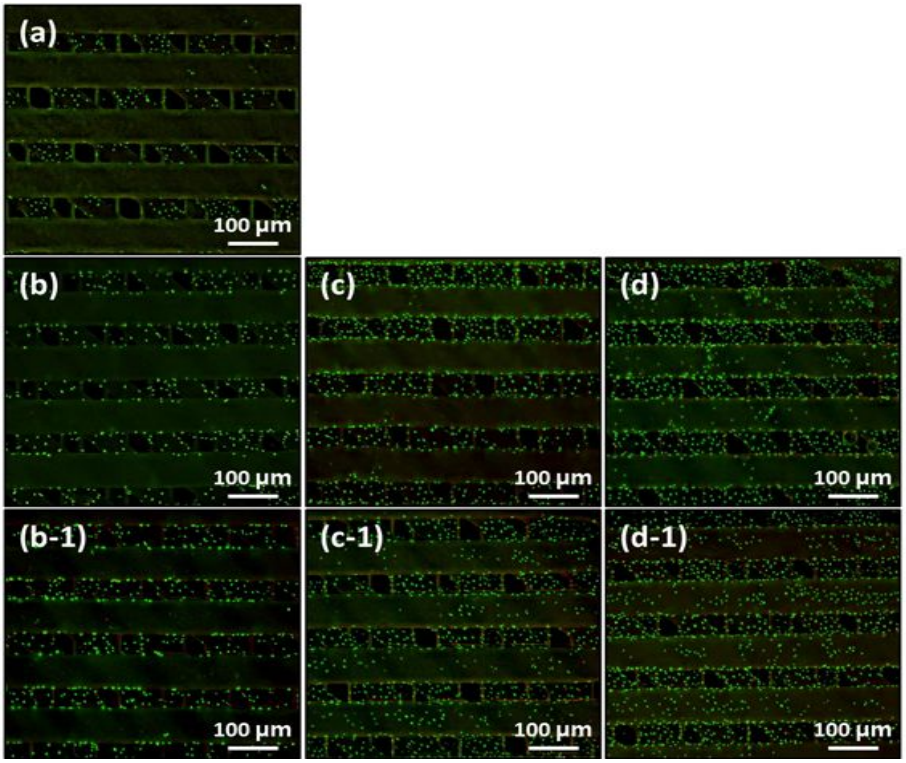

Fig. 20. Images of live/dead staining of the (a) pristine PCL scaffold, (b) PCL/PPAAc scaffold, (c) PCL/PPAAm scaffold, (d) PCL/DACH scaffold, (b-1) PCL/PPAAc/P24 scaffold, (c-1) PCL/PPAAm/P24 scaffold, and (d-1) PCL/DACH/P24 scaffold.

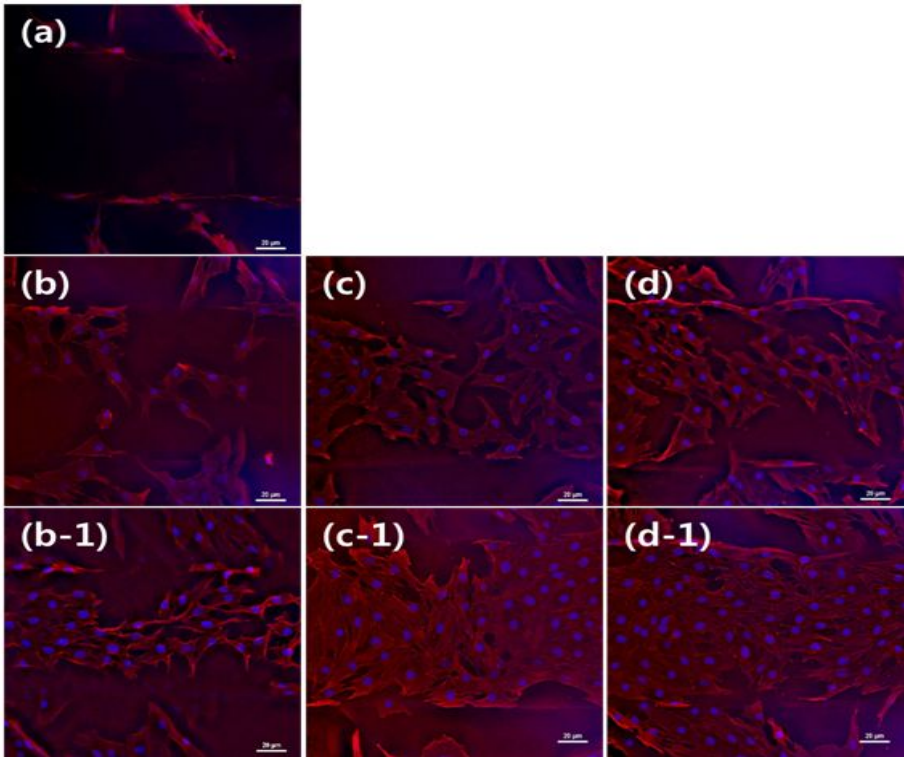

Fig. 21. Images of rhodamine-phalloidin staining of the (a) pristine PCL scaffold, (b) PCL/PPAAc scaffold, (c) PCL/PPAAm scaffold, (d) PCL/DACH scaffold, (b-1) PCL/PPAAc/P24 scaffold, (c-1) PCL/PPAAm/P24 scaffold, and (d-1) PCL/DACH/P24 scaffold. (scale bar : 20 μm)

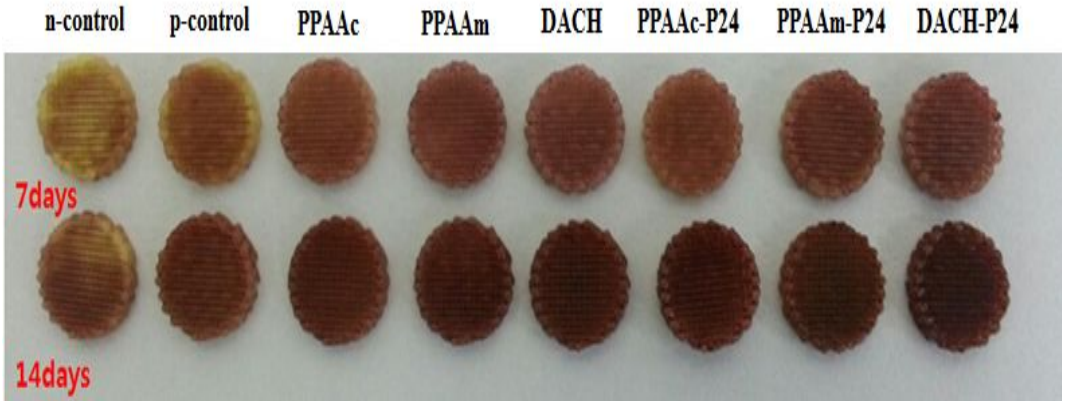

Fig. 22. Images of alizarin red S staining of the 3-D PCL scaffolds after 7 and 14 days.

Chapter 5. Conclusions

BMP-2 mimetic peptide immobilized biocompatibility material (3-D PCL scaffold) obtained the results of following as :

1. Biocompatible 3-D PCL scaffolds were fabricated using the 3-D printing method.

2. 3-D printing method provides a tool for precisely controlling the pore size and layer thickness.

3. The pristine PCL film exhibited a contact angle of 54.46° . On the other hand, the plasma-polymerized PCL film surface led to significant reduction in the angle 27.23° , 36.56° and 37.53° , owing to the hydrophilicity of the surface modification. The ATR-FTIR spectra of P24 immobilized groups were presenting characteristic absorption bands at 1639 and 1682 cm^{-1} (amide Ⅰ), 1528 and 1567 cm^{-1} (amide Ⅱ).

4. Favorable *in vitro* biocompatibility and osteogenic differentiation of the PCL scaffold were evidenced by continuously increasing cell proliferation.

5. The PCL/DACH/P24 surface modification improves the hydrophilic properties of the 3-D PCL scaffold, which is fundamental to support the cell behavior.

In present study, along with the published data, implied that the surface modification of PCL with P24 peptide advantageous for its practical application in tissue engineering.

Reference

Antreas Kantaros, Dimitris Karalekas (2013). Fiber Bragg grating based investigation of residual strains in ABS parts fabricated by fused deposition modeling process. *MATER. DESIGN.* **50**:44-50.

Anuja M. Rane, Sriramakamal Jonnalagadda, Zhitu Li (2013). On-column refolding of bone morphogenetic protein-2 using cation exchange resin. *PROTEIN. EXPRES. PURIF.* **90**:135-140.

BaoHong Zhao, weiming tian, Hailan Feng, In Seop Lee, FuZhai Cui (2005). Effects of RGD peptide grafting to titanium dental implants on the adhesion of human gingival fibroblasts and epithelial cells. *CURR. APPL. PHYS.* **5**:407-410.

Beatriz Veleirinho, Fernanda V. Berti, Paulo F. Dias, Marcelo Maraschin, Rosa M. Ribeiro-do-Valle, JoséA. Lopes-da-silva (2013). Manipulation of chemical composition and architecture of non-biodegradable poly(ethylene terephthalate)/chitosan fibrous scaffolds and their effects on L929 cell behavior. *MAT. SCI. ENG. C.* **33**:37-46.

Chul Ho Jang, Min Seong Kim, Yong Beom Cho, Yoon Seok Jang, Geun Hyung Kim (2013). Mastoid obliteration using 3D PCL scaffold in combination with alginate and rhBMP-2. *INT. J. BIOL. MACROMOL.* **62**:614-622.

D.A. Puleo, R.A. Kissling, M.-S. Sheu (2002). A technique to immobilized bioactive proteins, including bone morphogenetic protein-4 (BMP-4), on titanium alloy. *BIOMATERIALS* **23**:2079-2087.

Dave Mangindaan, Wei-Hsuan Kuo, Ching-Chuan Chang, Shu-Ling Wang, Hsiu-Chi Liu, Meng-Jiy Wang (2011). Plasma polymerization of amine-containing thin films and the studies on the deposition kinetics. *SURF. COAT. TECH.* **206**:1299-1306.

Dietmar W. Hutmacher, Thorsten Schantz, Iwan Zein, Kee woei NG, Swee Hin

teoh, Kim Cheng Tan (2001). Mechanical properties and cell cultural response of polycaprolactone scaffolds designed and fabricated via fused deposition modeling. *J. BIOMED. MATER. RES. A* **55**:203-216.

Dina Noff, Sandu Pitaru, Naphtali Savion (1989). basic fibroblast growth factor enhances the capacity of bone marrow cells to form bone-like nodules in vitro. *FEBS. LETT.* **250**:619-621.

Eric J. McCullough, Vamsi K. Yadavalli (2013). Surface modification of fused deposition modeling ABS to enable rapid prototyping of biomedical microdevices. *J. MATER. PROCESS. TECH.* **213**:947-954.

Farshid Sefat, Morgan C.T. Denyer, Mansour Youseffi (2014). Effect of different transforming growth factor beta (TGF-β) isomers on wound closure of bone cell monolayers. *CYTOKINE* **69**:75-86.

George D. Yancopoulos, Michael Klagsbrun, Judah Folkman (1998). Vasculogenesis, Angiogenesis and Growth Factors: Ephrins Enter the Fray at the Border. *CELL* **93**:661-664.

Girish Kumar, Christopher K. Tison, Kaushik Chatterjee, P.Scott Pine, Jennifer H. McDaniel, Marc L. Salit, Marian F. Young, Carl G. Simon Jr (2011). The determination of stem cell fate by 3D scaffold structures through the control of cell shape. *BIOMATERIALS* **32**:9188-9196.

Gupta B, Plummer C, Bisson I, Frey P, Hilborn J (2002). Plasma-induced graft polymerization of acrylic acid onto poly (ethylene terephthalate) films: characterization and human smooth muscle cell growth on grafted films. *BIOMATERIALS* **23**:863-71.

Heikki Tokola, Jaana Rysä, Sampsa Pikkarainen, Nina Hautala, Hanna Leskinen, Risto Kerkelä, Mika Ilves, Jani Aro, Olli Vuolteenaho, Olli Ritvos, Heikki Ruskoaho (2014). Bone morphogenetic protein-2 - A potential autocrine/paracrine factor in mediating the stretch activated B-type and atrial natriuretic peptide expression in cardial myocytes. *MOL.*

CELL.ENDOCRINOL. Article in press.

Hongbo Lan (2009). web-based rapid prototyping and manufacturing systems: A review. *COMPUT. IND.* **60**:643-656.

H. Senta, H. Park, E. Bergeron, O. Drevelle, D. Fong, E. Leblanc, F. Cabana, S. Roux, G. Grenier, N. Faucheux (2009). Cell responses to bone morphogenetic proteins and peptides derived from them: Biomedical applications and limitations. *CYTOKINE. GROWTH. F. R* **20**:213-222.

Hyeongjin Lee, Heon Hwang, Yeseul Kim, Hojun Jeon, GeunHyung Kim (2014). Physical and bioactive properties of multi-layered PCL/silica composite scaffolds for bone tissue regeneration. *CEHM. ENG. J* **250**:399-408.

Hyun-Uk Lee, Ye-Sul Jeong, Se-Young Jeong, So-Young Park, Jong-Seong Bae, Hyun-Gyu Kim, Chae-Ryong Cho (2008). Role of reactive gas in atmospheric plasma for cell attachment and proliferation on biocompatible poly ε-caprolactone film. *APPL. SURF. SCI.* **254**:5700-5705.

Hyun Suk Seo, Yeong Mu Ko, Jae Won Shim, Yun Kyong Lim, Joong Ki Kook, Dong Lyun Cho, Byung Hoon Kim (2010). Characterization of bioactive RGD peptide immobilized onto poly(acrylic acid) thin films by plasma polymerization. *APPL. SURF. SCI.* **257**:596-602.

Inés Sousa, Ausenda Mendes, Rüben F. Pereira, Paulo J. Bártolo (2014). Collagen surface modified poly(ε-caprolactone) scaffolds with improved hydrophilicity and cell adhesion properties. *MATER. LETT.* **134**:263-267.

Jae Gyoon Kim, Hak Jun Kim, Sung Eun Kim, Ji Hoon Bae, You Jin Ko, Jung Ho Park (2014). Enhancement of tendon-bone healing with the use of bone morphogenetic protein-2 inserted into the suture anchor hole in a rabbit patellar tendon model. *CYTOTHERAPY* **16**:857-867.

Jingfeng Li, Zhenyu Lin, Qixin Zheng, Xiaodong Guo, Shenghui Lan, Sunan Liu, Shuhua Yang (2010). Repair of rabbit radial bone defects using true bone

ceramics combined with BMP-2-related peptide and type I collagen. *MAT. SCI. ENG. C-MATER.* **30**:1272-1279.

Jing Zou, Jun Ma, Xiang Zhang, Pengchao Xie (2014). Rapid spectrophotometric determination of peroxymonosulfate in water with cobalt-mediated oxidation decolorization of methyl orange. *CHEM.ENG. J* **253**:34-39.

Kazuhiro Aoki, Neil Alles, Niroshani Soysa, Keiichi Ohya (2012). Peptide-based delivery bone. *ADV. DRUG. DELIVER. REV.* **64**:1220-1238.

Lauren B. Priddy, Ovijit chaudhuri, Hazel Y. Stevens, Laxminarayanan Krishnan, Brent A. Uhrig, Nick J. Willett, Robert E. Guldberg (2014). Oxidized alginate hydrogels for bone morphogenetic protein-2 delivery in long bone defects. *ACTA. BIOMATER.* **10**:4390-4399.

L.M. Galantucci, F.Lavecchia, G. Percoco (2010). Quantitative analysis of a chemical treatment to reduce roughness of parts fabricated using fused deposition modeling. *CIRP. ANN-MANUF. TECHN.* **59**:247-250.

Loredana Detomaso, Roberto Gristina, Giorgio S. Senesi, Riccardo d'Agostino, Pietro Favia (2005). Stable plasma-deposited acrylic acid surfaces for cell culture applications. *BIOMATERIALS* **26**:3831-3841.

Marc A. Fernandez-Yague, Sunny Akogwo Abbah, Laoise McNamara, Dimitrios I. Zeugolis, Abhay Pandit, Manus J. Biggs (2014). Biomimetic Approaches in Bone Tissue Engineering: Integrating Biological and Physicomechanical Strategies. *ADV. DRUG. DELIVER. REV* Article in press.

Maria C. Serrano, Maria C. Gutiérrez, Francisco del Monte (2014). Role of polymers in the design of 3D carbon nanotube-based scaffolds for biomedical applications. *PROG. POLYM. SCI.* **39**:1448-1471.

Marian H. Hettiaratchi, tobias Miller, Johnna S. Temenoff, Robert E. Guldberg (2014). Heparin microparticle effects on presentation and bioactivity of bone morphogenetic protein-2. *BIOMATERIALS* **35**:7228-7238.

Matthias Wiens, Tarek A. Elkhooly, Heinz-Christoph SchrÖder, Tawheed H.A. Mohamed, Werner E.G. Müller (2014). Characterization and osteogenic activity of a silicatein/biosilica-coated chitosan-graft-polycaprolactone. *ACTA. BIOMATER.* **10**:4456-4464.

Naveen Kumar Mekala, Rama Raju Baadhe, Sreenivasa Rao Parcha, Prameela Devi Yalavarthy (2013). Physical and degradation properties of PLGA scaffolds fabricated by salt fusion technique. *J. BIOMED. RES.* **27**:318-325.

Nurizzati Mohd Daud, Ng Boon Sing, Abdul Hakim Yusop, Fadzilah Adibah Abdul Majid, Hendra Hermawan (2014). Degradation and *in vitro* cell-material interaction studies on hydroxyapatite-coated biodegradable porous iron for hard tissue scaffolds. *J. ORTHOPAEDIC. TRANSLATION.* **2**:177-184.

Olivier Drevelle, Alex Daviau, Marc-Antoine Lauzon, Nathalie Faucheux (2013). Effect of BMP-2 and/or BMP-9 on preosteoblasts attached to polycaprolactone functionalized by adhesive peptides derived from bone sialoprotein. *BIOMATERIALS* **34**:1051-1062.

Omar F. Zouani, Jérôme Kalisky, Emmanuel Ibarboure, Marie-Christine Durrieu (2013). Effect of BMP-2 from matrices of different stiffnesses for the modulation of stem cell fate. *BIOMATERIALS* **34**:2157-2166.

Peng cai, Zhongyuan Xue, Wei Qi, Hua Wang (2013). Adsorbed BMP-2 in polyelectrolyte multilayer films for enhanced early osteogenic differentiation of mesenchymal stem cells. *COLLOID. SURFACE. A* **434**:110-117.

Qizhi Chen, George A. Thouas (2015). Metallic implant biomaterials. *MAT. SCI. ENG. R* **87**:1-57.

Roland M. Klar, Raquel Duarte, Therese Dix-Peek, Ugo Ripamonti (2014). The induction of bone formation by the recombinant human transforming growth factor-β_3. *BIOMATERIALS* **35**:2773-2788.

Roohollah Bagherzadeh, Masoud Latifi, Lingxue Kong (2014). Three-dimensional pore structure analysis of polycaprolactone nano-microfibrous scaffolds using theoretical and experimental approaches. *J. BIOMED. MATER. RES. A* **102**:903-910.

Ruchi Mishra, Ashok Kumar (2014). Effect of plasma polymerization onphysicochemical properties of biocomposite cryogels causing a differential behavior of human osteoblasts. *J. COLLOID. INTERF. SCI.* **431**:139-148.

Sarat Singamneni, Asimava Roychoudhury, Olaf Diegel, Bin Huang (2012). Modeling and evaluation of curved layer fused deposition. *J. MATER. PROCESS. TECH.* **212**:27-35.

Shalini Verma, Neeraj Kumar (2010). Effect of biomimetic 3D environment of an injectable polymeric scaffold on MG-63 osteoblastic-cell response. *MAT. SCI. ENG. C* **30**:1118-1128.

Shih-Hang Chang, Chin-He Chian (2013). Plasma surface modification effects on biodegradability and protein adsorption properties of chitosan films. *APPL. SURF. SCI.* **282**:735-740.

S. Sartori, A. Rechichi, G. Vozzi, M. D'Acunto, E. Heine, P. Giusti, G. Ciardelli (2008). Surface modification of a synthetic polyurethane by plasma glow discharge: Preparation and characterization of bioactive monolayers. *REACT. FUNCT. POLYM.* **68**:809-821.

Sung Woon Myung, Yeong Mu Ko, Byung Hoon Kim (2013). Effect of plasma surface functionalization on preosteoblast cells spreading and adhesion on a biomimetic hydroxyapatite layer formed on a titanium surface. *APPL. SURF. SCI.* **287**:62-68.

Shuqiong Liu, Zhihang He, guojie Xu, Xiufeng Xiao (2014). Fabrication of polycaprolactone nanofibrous scaffolds by facile phase separation

approach. *MAT. SCI. ENG. C-MATER.* **44**:201-208.

Thomas Billiet, Mieke Vandenhaute, Jorg Schelfhout, Sandra Van Vlierberghe, Peter Dubruel (2012). A review of trends and limitations in hydrogel-rapid prototyping for tissue engineering. *BIOMATERIALS* **33**:6020-6041.

Tracey Hanks, Brent Lee Atkinson (2004). Comparison of cell viability on anorganic bone matrix with or without P-15 cell binding peptide. *BIOMATERIALS* **25**:4831-4836.

Victor Multanen, Gilad Chaniel, Roman Grynyov, Ron Yossef Loew, Naor Kyle Siany, Edward Bormashenko (2014). Hydrophilization of liquid surfaces by plasma treatment. *COLLOID. SURFACE. A* **461**:225-230.

Wei-Chen Lee, Ching-Chih Wei, Shan-Chen Chung (2014). Development of a hybrid rapid prototyping system using low-cost fused deposition modeling and five-axis machining. *J. MATER. PROCESS. TECH.* **214**:2366-2374.

Xiangjun Kong, Jing Wang, Lingyan Cao, Yuanman Yu, Changsheng Liu (2014). Enhanced osteogenesis of bone morphology protein-2 in 2-*N*,6-O-sulfated chitosan immobilized PLGA scaffolds. *COLLOID. SURFACE. B* **122**:359-367.

Xue Qu, Wenjin Cui, Fei Yang, Changchun Min, Hong Shen, Jianzhong Bei, Shenguo Wang (2007). The effect of oxygen plasma pretreatment and incubation in modified simulated body fluids on the formation of bone-like apatite on poly(lactide-co-glycolide) (70/30). *BIOMATERIALS* **28**:9-18.

Xufeng Niu, Qingling Feng, Mingbo Wang, Xiaodong Guo, Qixin zheng (2009). *In vitro* degradation and release behavior of porous poly(lactic acid) scaffolds containing chitosan microspheres as a carrier for BMP-2-derived synthetic peptide. *POLYM. DEGRAD. STABIL.* **94**:176-182.

Xufeng Niu, Qingling Feng, Mingbo Wang, Xiaodong Guo, Qixin Zheng (2009). Porous nano-HA/collagen/PLLA scaffold containing chitosan microspheres for controlled delivery of synthetic peptide derived from BMP-2. *J. CONTROL.*

RELEASE. **134**:111-117.

Xu Wang, Yaping Wang, Li Li, Zhipeng Gu, Huizu Xie, Xixun Yu (2014). Stimulations of strontium-doped calcium polyphosphate for bone tissue engineering to protein secretion and mRNA expression of the angiogenic growth factors from endothelial cells *in vitro*. *CERAM. INT.* **40**:6999-7005.

Yeong-Mu Ko, Kang Lee, Byung-Hoon Kim (2013). Efferc of Functional groups on Biodegradation and Pre-osteoblastic Cell Response on the Plasma-Polymerized Magnesium Surface. *JPN. J. APPL. PHYS.* **52**:01AE01.

Yi Wu, Juan Hou, ManLi Yin, Jing Wang, changSheng Liu (2014). enhanced healing of rabbit segmental radius defects with surface-coated calcium phosphate cement/bone morphogenetic protein-2 scaffolds. *MAT. SCI. ENG. C-MATER.* **44**:326-335.

Young-Eun Cho, Ethel Alcantara, Santhy Kumaran, Kun-Ho Son, Ho-Young Sohn, Jong-Hwa Lee, Chung-Sig Choi, Tae-youl Ha, In-Sook Kwun (2010). Red yeast rice stimulates osteoblast proliferation and increases alkaline phosphatase activity in MC3T3-E1 cells. *NUTER. RES.* **30**:501-510.

Young Jun Lee, Ji Hye Lee, Hyeong Jin cho, Hyung Keun Kim, taek rim Yoon (2013). Electrospun fibers immobilized with bone forming peptide-1 derived from BMP7 for guided bone regeneration. *BIOMATERIALS* **34**:5059-5069.

Z.F. Lu, S.I. Roohani-Esfahani, J.J. Li, Hala Zreiqat (2014). Synergistic effect of nanomaterials and BMP-2 signalling in inducing osteogenic differentiation of adipose tissue-derived mesenchymal stem cells. *NANOMED-NANOTECHNOL.* Article in press.

Zhen-Yu Lin, Zhi-Zia Duan, Xiao-Dong Guo, Jing-Feng Li, Hong-Wei Lu, Qi-Xin Zheng, Da-Ping Quan, Shu-Hua Yang (2010). Bone induction by biomimetic PLGA-(PEG-ASP)n copolymer loaded with a novel sunthetic BMP-2-related peptide *in vitro* and *in vivo*. *J. CONTROL. RELEASE.* **144**:190-195.

Ziyuan Cheng, Swee-Hin teoh (2004). Surface modification of ultra thin poly (ε-caprolactone) films using acrylic acid and collagen. *BIOMATERIALS* **25**:1991-2001.

Zuwei Ma, ZhengWei Mao, Changyou Gao (2007). Surface modification and property analysis of biomedical polymers used for tissue engineering. *COLLOID. SURFACE. B* **60**:137-157.

Z.X. Duan, Q.X. Zheng, X.D. Guo, Q. Yuan, S.G Chen (2007). Experimental research on ectopic osteogenesis of BMP2-derived peptide P24 combined with PLGA copolymers. *J. Huazhong Univ. Sci. Technolog. Med. Sci* **27**:179-182.

- 감사의 글 -

대학원에 입학하여 여러모로 부족한 제가 대학원생활을 잘 끝마칠 수 있도록 이끌어주시고 도와주신, 많은 분들의 관심과 사랑이 이제는 사회에 한 발 더 내딛어 용기를 얻을 수 있는 경험들이었습니다. 본 논문이 잘 끝마칠 수 있도록 옆에서 지켜봐주시고 도와주신 교수님들과 선생님들, 그리고 실험실 식구들, 모든 분들께 감사의 인사를 드리고자 이 편지를 올립니다.

늘 한결 같은 마음으로 지도해주시고 부족한 제가 한층 성숙해질 수 있도록 관심과 사랑으로 보살펴주신 고영무 교수님, 최한철 교수님, 김병훈 교수님, 유영법 교수님께 먼저 진심으로 감사의 인사를 드립니다. 대학교를 졸업 후 대학원에 입학하기까지 짧으면 짧고, 길면 긴 2년 이라는 시간동안 친자식처럼 생각해주시고 강하게 클 수 있도록 지도해주신 김병훈 교수님, 유영법 교수님께 다시 한 번 감사의 인사를 드립니다.

실험실에서 생활하면서 많은 도움과 따뜻한 정을 베풀어 주신 모든 분들에게 너무나도 감사합니다. 먼저 우리 실험실 식구들.. 먼저 2년 동안 옆에서 함께 지내오며 항상 저에게 용기를 북 돋아주시고 아울러 연구방향을 함께 제시해주시고 도와주신 명성운 박사님, 최도영 박사님께 감사의 인사를 드립니다. 그리고 부족한 저의 부분을 채워주시고, 세포실험에 있어 많은 도움을 주신 황영현 선생님, 실험실의 전반적인 일을 도맡아 주신 황영선 선생님께도 깊은 감사의 인사를 드립니다.

친형 같았고 그리고 많은 추억을 만들어갔던 우리 희상이형, 나의 하나밖에 없는 동기 태영이와 채익이, 대학교 후배이자 대학원 후배인 나랑 비슷한 우리 수영이, 그리고 세차도 같이 하며 많은 짓궂은 장난도 같이 치며 지내온 우리 영욱이 형에게도 너무나도 많은 감사를 드립니다.

변함없는 벗을 이어가고 있는 청주의 친구들과 오랜 시간 함께한 진희에게도 항상 뒤에서 힘을 주어서 너무나도 힘이 났고 그로인해 유종의 미를 거둘 수 있었습니다.

그리고 마지막으로, 저를 이 세상에 태어나게 해주시고 사랑과 정성으로 키워주신, 항상 내 편이 되어 주신 우리 부모님, 그리고 하나밖에 없는 형에게 너무나도 깊은 감사의 인사를 드리고 싶습니다. 하나 밖에 없는 우리 가족, 그 가족의 중앙에서 항상 꿋꿋하게 지켜올 수 있게 해주신 가장인 아버지, 힘들 때 항상 먼저 생각나는 포근하고 따뜻한 우리 어머니, 힘이 들 때면 같이 술 한 잔 기울이며 진솔한 이야기를 나눌 수 있는 친구 같은 나의 형, 언제나 변함없이 사랑합니다.

다시 한 번 모든 분들께 고개 숙여 깊은 감사의 인사를 드리며 이 글을 끝마치겠습니다. 감사하고 사랑합니다.

2014 년 12 월

신 건 수 올림.